Earth and Planetary Science Letters

Seismically induced kinking in quartz

--Manuscript Draft--

Manuscript Number:	EPSL-D-24-01199
Article Type:	Letters
Keywords:	quartz; kinking; seismic; athermal dislocation; anisotropy; weighted Burgers vector
Corresponding Author:	Michel Bestmann University of Vienna Vienna, AUSTRIA
First Author:	Michel Bestmann
Order of Authors:	Michel Bestmann
	Bernhard Grasemann
	Rüdiger Kilian
	John Wheeler
	Luiz F.G. Morales
	Andreas Bezold
	Giorgio Pennacchioni
Abstract:	Deformed quartz veins next (1-1.5m) to an exhumed pseudotachylyte-bearing (i.e. anciently seismic) fault within the Schobergruppe (Austroalpine Crystalline Complex, Eastern Alps) contain intensely kinked quartz grains. The monoclinic symmetry of kink bands is consistent with the slip sense of the fault. Cathodoluminescence images show a very high density of intragranular, sub-planar, lamellae accompanied by nanometre-scale fluid-related porosity visible in electron backscatter orientation contrast. Based on the oscillating orientation variation across subgrain boundaries (misorientation angle 1-9°) these lamellae (oriented (sub)parallel to a rhomb plane and spaced 4-10 µm apart) are identified as short-wavelength undulatory extinction microstructures (SWUE). Transmission electron microscopy reveals a high degree of recovery (low dislocation density) across the SWUE. Only grains with SWUE oriented parallel to the vein boundary are kinked. We infer following history for the kink evolution related to the seismic cycle: (I) Deformation lamellae formed during high differential stresses preceding the earthquake rupturing or associated with seismic rupture propagation. The initial high dislocation density within the deformation lamellae provided the mechanical anisotropy in quartz required for (II) the subsequent coseismic initiation of kinking. The lamellae acted as a geometric filter that only allowed r<a> slip of dislocations parallel to the lamellae. These athermal dislocations were able to glide fast over a relatively large distance before piling up and initiating kinking during the coseismic event. Progressive build-up of dislocations resulted in deformation bands which accumulated the final misorientation angle between host domain and kink domain. (III) During post-seismic deformation dislocations were dynamically re-arranged under residual stress into sub-parallel subgrain boundaries which now characterize the kink band boundary region. We suggest that kinking in quartz potentially indicates coseismic deformation and is an important mechanism for incipient strain accommodation during high strain rates.
Suggested Reviewers:	Claudia Trepmann Ludwig Maximillians University Munich claudia.trepmann@lmu.de specialist in rock deformation, impact research, structural geology, paleo-seismology, SEM + TEM analytic
	Thomas Kenkmann Albert-Ludwigs-Universität Freiburg thomas.kenkmann@geologie.uni-freiburg.de Specialist in impact researcher and structural geology, TEM analytic

	Dave Prior University of Otago - Dunedin Campus david.prior@otago.ac.nz Specialist in structural geology, rock deformation, paleo-seismology, SEM analytic
	Martyn Drury Utrecht University M.R.Drury@uu.nl Specialist in structural geology, rock deformation, impact research, SEM + TEM analytic
	Sandra Piazolo University of Leeds S.Piazolo@leeds.ac.uk specialist in structural geology, rock deformation, impact research, paleo-seismology, EBSD
Opposed Reviewers:	

Cover Letter

University of Vienna
Department of Geology

Michel Bestmann
Josef-Holaubek-Platz 2/UZAII
A1090 Vienna (Austria)

T +43 1 4277 53611
EMAIL michel.bestmann@univie.ac.at

Earth and Planetary Science Letters

Vienna 09.09.2024

Dear Editor,

We hereby submit a "letter" manuscript to Earth and Planetary Science Letters titled "*Seismically induced kinking in quartz"* by Bestmann, Grasemann, Kilian, Wheeler, Morales, Bezold and Pennacchioni. This paper focuses on detailed microstructural analyses of a deformed quartz vein next to a seismic fault zone. Our results provide insights about the deformation processes of kinking in quartz related to the seismic cycle. We were able to show that at the initial state of the seismic cycle pervasive formation of deformation lamellae provided the mechanical anisotropy necessary for subsequent coseismic kinking in quartz. In recent years, kinking in minerals, e.g. mica, ice and also alloys were of particular interest as an important deformation process in general, and in particular related to seismicity and meteorite impact. Therefore, our finding is of broad interest to a large swath of geoscientists.

In this paper, we applied, for the first time, an integrated microstructural analysis workflow by correlated microscopy by using optical microscopy, scanning electron microscopy cathodoluminescence, electron backscatter diffraction (including weighted Burgers vector analysis), and transmission electron microscopy on a well-developed kinking in quartz. The association of the kinked quartz with a pseudotachylyte-bearing fault allows the development of quartz kinking to be discussed in the frame of the seismic cycle. In our model deformation lamellae formed at transient high differential stresses either during the loading stages preceding the earthquake or associated with the seismic rupture propagation. The initial high dislocation density within the deformation lamellae provided the mechanic anisotropy in quartz required for the subsequent coseismic initiation of kinking by fast slip of athermal dislocations. During post-seismic deformation dislocations were dynamically re-arranged under residual stress into sub-parallel subgrain boundaries which now characterize the kink band boundary region.

We believe our paper is of special interest to the readers of EPSL, for several reasons. It has appeal for a variety of earth scientists, from structural geologist to paleo-seismologist to meteorite impact researchers, and for material

scientists. Our results show that transient high differential stress can produce an internal effective mechanical anisotropy even in a strong mineral like quartz which normally is free of weak crystallographic planes necessary for kinking. Surprisingly, subsequent crystal plastic processes can occur in a very short time span during coseismic deformation (possibly within milliseconds) even at relatively low ambient temperatures (300-350 °C) and relatively high strain rates in combination with still persisting high differential stresses. Therefore, intensive kinking of quartz potentially indicates paleoseismicity and is an important process of initial strain accommodation in crystals during coseismic high differential stress.

We also would like to suggest a selection of potential reviewers, all of which are experts in the areas of either structural geology, paleo-seismology, impact researchers or a combination thereof:

Claudia Trepmann	claudia.trepmann@lmu.de	University Munich
Thomas Kenkmann	thomas.kenkmann@geologie.uni-freiburg.de	University Freiburg
Dave Prior	david.prior@otago.ac.nz	University Otago
Martyn Drury	M.R.Drury@uu.nl	Utrecht University
Sandra Piazolo	S.Piazolo@leeds.ac.uk	University of Leeds

We confirm that: (i) the data, results, and conclusions presented in this paper are original; (ii) this manuscript has not been published elsewhere and is not under consideration by another journal; and (iii) all authors have approved the manuscript and agree with its submission to Earth and Planetary Science Letters. Our submission includes 9 figures, a manuscript with a word count less than the maximum allowable, and supplementary material.

We thank you very much for your consideration, and look forward to further correspondence.

Sincerely,
Michel Bestmann (corresponding author)
Bernhard Grasemann
Rüdiger Kilian
John Wheeler
Luiz Morales
Andreas Bezold
Giorgio Pennacchioni

Highlight (3-5 bullet points, each max. 85 characters incl spaces)

- High transient differential stress produced deformation lamellae in quartz
- Initial high dislocation density in deformation lamellae cause mechanical anisotropy
- Deformation lamellae act as a geometric filter for dislocations slip
- Seismically induced athermic dislocations glide fast and initiate kinking
- Intense quartz and mica kinking can indicate coseismic deformation

Seismically induced kinking in quartz

Michel Bestmann[1],

Bernhard Grasemann[1],

Rüdiger Kilian[2],

John Wheeler[3],

Luiz F.G. Morales[4],

Andreas Bezold[5],

Giorgio Pennacchioni[6]

[1]University of Vienna, Department of Geology, Vienna, Austria

[2]University of Halle, Department of Geosciences and Geography, Halle, Germany

[3]University of Liverpool, Department of Earth, Ocean and Ecological Sciences, Liverpool, United Kingdom

[4]ETH Zürich, ScopeM, Zürich, Switzerland

[5]FAU Erlangen-Nürnberg, Germany, Department of Materials Science and Engineering (WW1), Erlangen, Germany

[6]University of Padova, Department of Geosciences, Padova, Italy

Corresponding author: michel.bestmann@univie.ac.at

Abstract

Deformed quartz veins next (1-1.5m) to an exhumed pseudotachylyte-bearing (i.e. anciently seismic) fault within the Schobergruppe (Austroalpine Crystalline Complex, Eastern Alps) contain intensely kinked quartz grains. The monoclinic symmetry of kink bands is consistent with the slip sense of the fault. Cathodoluminescence images show a very high density of intragranular, sub-planar, lamellae accompanied by nanometre-scale fluid-related porosity visible in electron backscatter orientation contrast. Based on the oscillating orientation variation across subgrain boundaries (misorientation angle 1-9°) these lamellae (oriented (sub)parallel to a rhomb plane and spaced 4-10 µm apart) are identified as short-wavelength undulatory extinction microstructures (SWUE). Transmission electron microscopy reveals a high degree of recovery (low dislocation density) across the SWUE. Only grains with SWUE oriented parallel to the vein boundary are kinked. We infer following history for the kink evolution related to the seismic cycle: (I) Deformation lamellae formed during high differential stresses preceding the earthquake rupturing or associated with seismic rupture propagation. The initial high dislocation density within the deformation lamellae provided the mechanical anisotropy in quartz required for (II) the subsequent coseismic initiation of kinking. The lamellae acted as a geometric filter that only allowed *r<a>* slip of dislocations parallel to the lamellae. These athermal dislocations were able to glide fast over a relatively large distance before piling up and initiating kinking during the coseismic event. Progressive build-up of dislocations resulted in deformation bands which accumulated the final misorientation angle between host domain and kink domain. (III) During post-seismic deformation dislocations were dynamically re-arranged under residual stress into sub-parallel subgrain boundaries which now characterize the kink band boundary region. We suggest that kinking in quartz potentially indicates coseismic deformation and is an important mechanism for incipient strain accommodation during high strain rates.

Keywords: quartz, kinking, seismic, athermal dislocation, anisotropy, weighted Burgers vector

1. Introduction

Recognition of seismically induced structures is important to unravel the different deformation processes during the seismic cycle, especially at the base of the upper brittle crust where many earthquakes nucleate. The ancient seismicity of an exhumed fault is commonly recognized by the occurrence of pseudotachylytes, i.e. quenched melts produced during seismic slip along the host fault (Cowan, 1999). However, other microstructures have been proposed to develop during seismic faulting, e.g. intensely kinked micas (White, 2001; Bestmann et al., 2011; Anderson, 2021). In this study, we describe a quartz vein, sampled at a distance of 1-1.5 m from a pseudotachylyte-bearing fault that shows intense kinking of the quartz grains. The mica-rich host rock of the vein also shows intense kinking of micas. Since quartz does not commonly have a strong mechanical anisotropy, we address the question of why and how kinking of quartz may develop. Kinking requires the presence of a planar mechanical anisotropy, e.g. a multi-layered structure with a regular periodic alternation of thin weakly bounded layers (or of high viscosity layers interleaved with thin low viscosity ones) such as in minerals with a strong cleavage, e.g. micas (Bell et al., 1986) or in industrial metallic nano-laminates (Zhang et al., 2022). Several experiments and numerical models have been carried out to understand the kinking process in foliated rocks (Gay and Weiss, 1974), micas (Bell et al., 1986) and metals (Humphreys et al., 2017; Zhang et al., 2022). Kinking is also observed within phases with a well-defined layer structure, e.g. kyanite, enstatite, and ice (i.e. Seidemann et al., 2020 and references within), and also in minerals with several slip systems, such as olivine and pyrite (compiled by Vernon, 2018) and mostly hexagonal metals (Matsumoto et al., 2018). Further, Cook et al. (2024) pointed out the importance of kinking to suppress strain hardening by localized strain accumulation in polycrystalline alloys. Compared to those phases where kinking is frequently observed, quartz with its three-dimensional covalent bonding does not show any particularly weak crystallographic plane or direction that could provide the mechanical anisotropy necessary for kinking. Interestingly, kinking in quartz was only observed in combination with deformation lamellae in naturally deformed quartz

(Nishikawa and Takeshita, 1999; Menegon et al., 2008) and in experiments (Carter et al., 1964). In recent studies on ice, electron backscatter diffraction (EBSD) analysis (including Weighted Burgers Vector analysis, WBV, Wheeler et al., 2009, 2024) has shown that kinking is an important mechanism of strain accommodation in crystals during the initial state of deformation under high differential stress (Piazolo et al., 2015; Seidemann et al., 2020). Our aim here is to present, for the first time, an integrated analysis by using EBSD (including WBV analysis), scanning electron microscopy (SEM) cathodoluminescence (CL) and transmission electron microscopy (TEM) on well-developed kinked quartz. The association of the kinked quartz with a pseudotachylyte-bearing fault allows to discuss the development of kinking with respect to the seismic cycle.

2. Geological Settings

The studied samples are deformed quartz veins from the pre-Alpine eclogite-facies paragneisses of the Austroalpine Prijakt Nappe of the Eastern Alps, Austria (Fig. 1a) (Schulz, 1993; Hauke et al., 2019). The quartz veins, parallel to the main foliation of the paragneisses (Fig.1b and c), underwent deformation under amphibolite-facies conditions (Linner, 1999) and were later affected by deformation during slip on a nearby E-W-striking, steeply-dipping, strike-slip fault also parallel to the main host-rock foliation. The fault zone, up-to-2 m wide, consists of cataclasites, ultracataclasites and pseudotachylytes (Fig. 1d). Within a distance of up to 4-5 m from the fault, the foliation-parallel quartz veins in the paragneiss were exploited by ductile (viscous) deformation at temperatures of 300-350 °C (Bestmann et al., 2021) forming locally mylonites. This ductile overprint is absent in veins more distant from the fault.

3. Methods

Thin sections were made from sample chips cut orthogonal to the quartz vein boundary and host rock foliation (subparallel to the fault zone boundary) (XZ section), and parallel to the mineral

stretching lineation (X direction). The orientation of kink band boundaries (KBBs) and short-wavelength undulatory extinction microstructures (SWUE, see *section 6.2.1*) were measured with a universal stage microscope. Backscatter electron orientation contrast (BSE-OC) images and EBSD measurements were performed with a Thermo Fischer Scientific (TFS) Helios nanoLab 600i field emission gun (FEG) SEM at the Department Materials Science and Engineering of the Friedrich-Alexander-University (FAU) Erlangen-Nürnberg. For EBSD analysis (step size 250 nm), an Oxford Instruments Symmetry detector was used in combination with the AZtec 4.3 software. CL images were captured with a panchromatic (185–850 nm) TESCAN CL detector attached to a TESCAN Vega-XM-U (tungsten filament) SEM at the GeoZentrum, FAU Erlangen-Nürnberg. Additionally, three CL images of representative microstructures were taken, using (i) the red filter, (ii) the green filter and (iii) the blue filter on a Gatan MonoCL4 system (wavelength sensitivity 185-850 nm) attached to a ZEISS Merlin FEG-SEM at the Department of Geosciences, Arctic University of Norway, Tromsö, Norway. Focussed ion beam (FIB) preparation of TEM samples, cut perpendicular to the thin section plane, was carried out at ScopeM at the ETH Zürich, Switzerland, using a TFS Helios nanoLab 600i FIB-SEM and TFS Helios-5-UX with an AutoTEM-5 system. TEM analysis were performed using a Phillips CM-200 with 200 kV at the Institute I: General Materials Properties of the Department of Materials Science and Engineering, FAU Erlangen-Nürnberg.

The EBSD data are presented as orientation maps (colour coded with respect to a specific sample reference direction) and the crystallographic directions and pole to crystal planes as pole figures with respect to the sample reference system, PF_s (XZ, Y-direction in the centre, coinciding with the vorticity axis). EBSD data were processed using Channel-5 (Oxford Instruments) and Mtex (https://mtex-toolbox.github.io/). Calculated misorientation axis for different misorientation angle intervals are presented in (i) crystallographic coordinates (IPF_c) and (ii) as pole figures in sample coordinates (PF_s). They give insights into what sorts of dislocations have accumulated in particular boundaries, but usually by assuming a single slip system and pure tilt boundaries (Neumann, 2000). To go beyond that assumption Weighted Burgers Vector were calculated using the Crystalscape

software (Wheeler et al., 2009, 2024). For further detailed information about sample preparation, acquisition parameters and data processing see Method section in supplemental material.

4. Samples

The analysed thin section is from a deformed quartz vein (HS-2017-4, UTM33 326574E/ 5198989N), 4-5 cm in thickness, where the vein crystals were stretched to strongly elongated grains (with an aspect ratio of as much as 6:1) during an earlier (pre-seismic) stage of ductile deformation (Bestmann et al., 2021). The long axis of elongated grains is oriented slightly oblique to the vein boundary indicating dextral sense of shear (top-to-E) in accordance with the kinematics of the strike-slip fault. Characteristic is the intense kinking of individual quartz grains across the entire thin section (Fig. 2a). The host-rock paragneiss, in direct contact with the vein, also shows strongly kinked micas (HS-2017-4b, Fig. 1c).

Five different quartz kink microstructures were analysed by optical microscopy, SEM-CL, EBSD and BSE-OC images. We describe here the most prominent and well-developed quartz kink microstructure. While the general conclusions are valid for all analysed kink microstructures, they can have slightly different characteristics (SOM-Fig. 1).

5. Results

5.1 Quartz kink microstructure

We first describe lamellae within kinked quartz grains, then the kink band boundary regions (KBBR).

5.1.1 Lamellae

In this contribution we use the word “lamellae” in a non-genetic way unless in the phrase “deformation lamellae”. Later we argue that the lamellae were once deformation lamellae but are now modified into SWUE (*section 6.2.1*). CL images reveal locally pervasive, dark lamellae (Fig. 2c) in most of the grains (either kinked or not, SOM-Fig. 1b, d). Lamellae are only visible in the blue spectral range (400-500 nm) while in the green (500-575 nm) or red spectral (600-700 nm) no CL intensity variation can be observed. Only the grains where the lamellae are oriented (sub)parallel to the vein boundary, here referred to as horizontal lamellae, are intensively kinked. The lamellae are very subtle under the optical microscope. The spatial density and sharpness of the lamellae in CL vary with their orientation: (i) the horizontal lamellae are sharply defined and closely spaced (3-10 μm apart); (ii) the inclined lamellae have a larger spacing (10-14 μm) and the dark/dull CL signal is blurred (Fig. 2c). We infer that the horizontal lamellae are in their original orientation (host domain) and were rotated in the oblique orientation during kinking (kink domain). The angle ψ between the horizontal and the inclined lamellae is 33-43°, and the angle φ between horizontal lamellae and KBBRs is 48-62° which is systematically smaller than the angle φ_k between the KBBRs and the inclined lamellae (75-90°) (Fig. 3). KBBRs also appear as dark features in CL.

In EBSD maps (Fig. 4a, b) low angle boundaries (LABs, <10° misorientation angle), also visible in BSE-OC images, match the horizontal lamellae (Fig. 5a-c). The misorientation angle across the lamellae is mainly in the range of 1-3°, with local values up to 5-9°. BSE-OC and light optical images show the presence of pores along LABs (Fig. 5b). Misorientation axes of LABs bounding horizontal lamellae cluster around the crystallographic *c*-axis <*0001*> (Fig. 4c). U-stage measurements show that the lamellae are oriented (sub)parallel to one of the *r* {*10-11*} planes (Fig. 5d-VI). Lamellae (sub)parallel to the basal plane, with misorientation axes clustering around *m* {*10-10*} or *a* <*11-20*>, are also observed (SOM-Fig. 1g). Here, we focus on the microstructure with lamellae subparallel to {*r*}. The angles between the misorientation axes and the traces of LABs ranges between 40° and 60° (Fig. 5h). WBVs (weighted averages of local Burgers vectors) point in opposite directions on the long boundaries of lamellae which are connected via a loop (Fig. 5d-III, V) and cluster around one of the

m-poles (Fig. 5d-IV). TEM-FIB foils across the lamellae reveal in general a very low dislocation density (Fig. 6a). Some of the LABs show evidence of ordered dislocations indicative of subgrain boundaries (SGBs), while others are relatively narrow and sharp without internal dislocation structure.

5.1.2 Kink bands and their boundary regions (KBBRs)

KBBRs have a dominant inclination angle β of 28-42° to the Z-direction, inclined consistently with the dextral slip of the nearby fault (Bestmann et al., 2021) (Fig. 2). The width of the alternating kink bands varies between 30-240 µm. KBBRs show a gradual orientation change and include: (i) a relatively wide zone (10-30 µm) containing mostly (sub)parallel LABs with a misorientation of 1-4.5°; and (ii) a narrower zone (< 10 µm) containing internal high angle grain boundaries (iHAGB) of 10-20°, locally up to 25° (Figs. 4c-II, 5c, 5e-g). Misorientation angle profiles indicate that LABs accommodate a cumulative misorientation angle of 33-43° across the KBBRs with a continuous orientation dispersion path (Bestmann and Prior, 2003) (Fig. 5g). The rotation axis is located around the Y-direction and corresponds to one of the poles to {*z*} or {π'} even for iHAGB (Figs. 4c-II, 5e, f). The continuous dispersion path defines a dextral sense of shear across KBBRs, considering the host as the reference orientation (Fig. 5e-VI, 5f-VI). The trace of KBBRs together with U-Stage measurements indicate that the KBBRs are (sub)parallel to one of the {*m*} planes (Fig. 5e-VI, 5f-VI). In contrast to horizontal LABs outside of the tilted domain, the misorientation axes of LABs within KBBRs cluster close to the crystallographic {*z*} and {π'} poles even for iHAGB (Figs. 4c-II, 5e-VII, 5f-VII). Misorientation axes cluster around the Y-direction. The angle between the misorientation axis and the trace of LABs is 0-10° (Fig. 5h). Therefore, the misorientation axis lays within the KBBR plane. Maps show the WBVs plot in opposite directions for the corresponding KBBRs (Fig. 5e-V, 5f-V). In the PF_s for the left KBBR ($KBBR_A$) the Burgers vectors plot towards the upper left quadrant (Fig. 5e-V) and for the right KBBR ($KBBR_B$) to the lower right quadrant (Fig. 5f-V). This can be explained by realising that the LABs bounding the kink bands are of opposite rotation sense on opposite sides of the bands.

WBVs have a maximum nearly perpendicular to the trace of the KBBRs, but with some scatter. In the IPF_c the Burges vectors are dispersed between *a* and *m* (Fig. 5e-IV, 5f-IV). The dislocation density is slightly higher across KBBRs (Fig. 6b) as for the horizontal lamellae in the host domain (Fig. 6a). Some LABs show internal ordered dislocations suggesting that they are subgrain boundaries whereas others do not show clear evidence of internal dislocations.

The tilted lamellae within the kinked domains visible in CL images cannot be detected in EBSD maps and BSE-OC images. However, at the margin towards KBBRs some relicts of former horizontal LABs, now slightly bent, are present (Figs. 4b, 5c, 5g). In the kink domain, LABs run parallel to KBBRs and have misorientation angles of 1.5-4.5°. Misorientation axes show two clusters: one parallel to {*c*} (relics of horizontal lamellae) and one parallel to the poles of {*z*} or {π'} (related to the KBBR low angle boundaries). PF_s show two clusters, one in the centre (KBBRs) and another around the position of the rotated *c*-axis (horizontal LABs) of the kink domain (Fig. 4c-III). The porosity along the CL lamellae is not evident in the kinked domains (Fig. 5b).

5.2 Microshear zones related to kinked quartz

The kinked grains are crosscut by (sub)horizontal intra-crystalline microshear zones and/or a bordered by inter-crystalline microshear zones (SOM-Fig. 2a, b). The recrystallized new grains have (i) a grain size of 2-6 µm (area equivalent diameter), similar to that of the subgrains (SOM-Fig. 2), and (ii) a crystallographic orientation progressively misoriented from that of the host grain (Bestmann et al., 2021). These features indicate dynamic recrystallization by subgrain rotation (Drury and Urai, 1990; Bestmann and Prior, 2003).

5.3 Mica kinking

Next to the kinked quartz vein the main foliation of the host rock paragneisses is delineated by mica layers of as much as 1 mm thickness (sample HS-2017-4b; Fig. 7a). Especially in these mica layers, muscovite and biotite show extensive kinking with different kink orientation (7b-d). Various types of kink bands are formed: (i) primary kink bands, (ii) secondary kink bands, and (iii) second generation of kink bands (sensu Etheridge et al., 1973). Characteristic are opening gaps between basal cleavage planes (Fig. 7h). The geometry of primary kink bands was analysed as potential indicator of coseismic loading (Anderson et al., 2021) (SOM-Fig. 3).

6. Discussion

In the following, we will relate the kinked quartz to the seismic cycle, where precursory or coseismic high differential stress conditions promoted the development of pervasive deformation lamellae. Lamellae introduced a strong mechanical anisotropy allowing subsequent coseismic initiation of kinking. Kinking was followed by dynamic recovery during post-seismic creep. Before discussing the deformation mechanisms (*section 6.2*) and the evolution model of quartz kinking (*section 6.3*), we briefly focus on mica kinking as evidence of coseismic deformation.

6.1 Coseismic kinking of micas

Kinking of micas has been described in several host rocks of pseudotachylyte-bearing faults (White, 2001; Bestmann et al., 2011, Anderson, 2021). Kinking can be evidence for the high differential stress transients in the host rock of a seismic fault related to the stage of earthquake rupture propagation immediately preceding seismic fault slip (Di Toro et al., 2005; Okubo et al., 2019; Mancktelow et al., 2022; Toffol et al., 2024). Anderson et al. (2021) suggested that the separation along the basal cleavage planes of micas, also observed in the rocks studied here (Fig. 7h), is characteristic for fast (coseismic) strain rates and contrast with the absence of separation in mica kinks developed under long-term geological strain rates. Further, the kink geometry also points to seismically produced

kinking (SOM-Fig. 3). Nearly pure mm thick mica layers seem to be prone to accommodate strain by instantaneous kinking even during the coseismic short-lived transient high differential stresses and strain rates. Aslin et al. (2019) showed that beside dislocation glide named ripplocations play a significant role for slip on (001). Instantaneous kinking of mica also occurs during impact events (Ebert et al., 2021 and references within) and nuclear explosions (Short, 1966) and therefore, it is likely that kinking could develop during seismic rupture events. Since the fault zone is (sub)parallel to the main foliation of the adjacent Schober paragneisses, and the (001) of mica are parallel to that foliation plane, the mica layers were in a favourable orientation for kinking during the seismic event. Honea and Johnson (1976) and Nishikawa and Takeshita (1999) showed that kinking mainly developed at high differential stress deformation when the maximum principal stress direction is roughly within the plane of mechanical layering. Therefore, the mica layer was able to accommodate the deformation by internal kinking. The different orientation of KBBs and the abundant appearance of secondary kink bands together with second generation of kink bands points to multiple kinking to accommodate larger strain (Etheridge et al., 1973).

6.2 Quartz deformation mechanisms and processes during the seismic cycle

6.2.1 Vein-parallel (horizontal) deformation lamellae in quartz

Quartz across the entire thin section shows pervasive lamellae identified by CL contrast, but only the grains with fault-parallel (horizontal) lamellae are intensively kinked. The lamellae contain numerous tiny fluid-related porosity reminiscent of those commonly described for deformation lamellae (White, 1973; Vernooij and Langenhorst, 2005). Deformation lamellae are crystallographically controlled narrow planar features with a spacing of 0.5 – 10 µm (Drury, 1993). Quartz deformation lamellae are commonly characterized by an initial high dislocation density (Christie et al., 1964; McLaren et al., 1970; Drury, 1993; Trepmann and Stöckhert, 2013) and show after subsequent recovery a small misorientation angle of 1-3° (Drury, 1993) to 4° (Vernooij and Langenhorst, 2005). In

contrast, the studied lamellae show very low dislocation density and misorientation angles up to 9°. Based on the oscillating orientation variation these lamellae are referred as short-wavelength undulatory extinction microstructures - SWUE (Trepmann and Stöckhert, 2013). In *kick-and-creep* deformation experiments (Trepmann and Stöckhert, 2013) of quartz the SWUE preserve evidence of an initial coseismic peak stress event (*kick* stage at 400 °C and 10^{-4} s^{-1} strain rate). The *kick* stage of the experiment produced a layering formed by basal deformation lamellae with a high density of tangled dislocations in alternation with domains of lower dislocations density characterized by a small misorientation angle (< 2°). In the secondary *creep* stage of the experiment (900-1000 °C at residual stress), dynamic recovery rearranged the high dislocation density of the deformation lamellae into SGBs, spaced ~10 µm, and caused the development of SWUE. The SWUE in our study are interpreted in a similar way. The initially high dislocation density within deformation lamellae caused a strong mechanical anisotropy within quartz crystals (Fig. 8-I). Tangled dislocations within deformation lamellae (McLaren et al., 1970) caused work hardening because of the increasingly restricted glide of dislocation on the slip plane (Durinck et al., 2007; Trepmann and Stöckhert, 2013; Humphreys et al., 2017). This produced a rheological contrast between the deformation lamellae with a high dislocation density (Christie et al., 1964; McLaren et al., 1970; Trepmann and Stöckhert, 2013), and the domains in between with a lower dislocation density. Therefore, deformation was mainly accommodated by slip of dislocations in the domains between the deformation lamellae.

The lower CL intensity of SWUE can be related to various reasons amongst others, e.g. elimination of CL-emitting structural defects or changes in trace element chemistry. Given that blue (~420nm) CL emissions in exactly the same vein quartz has been attributed to Ti^{4+} (Bestmann et al., 2021), a loss of emission in SWUE could indicate either loss of Ti^{4+} or at least reordering those Ti^{4+} defects into a non-emitting state. Drury (1993) pointed out that the variation of fluid-related pore density along SGBs can reflect inhomogeneous recovery. In the studied vein, fluids could have derived from decrepitation of fluid inclusions during the initial deformation of the original vein crystals (Tarantola et al., 2010), resulting in the irregular traces of porosity observed along the SWUE

(Fig 5b). Subsequently, the high dislocation density along deformation lamellae could have facilitated fluid infiltration (Carter et al., 1964; Drury, 1993) and modification of Ti^{4+} defects such that total CL emission is reduced. At the other hand, post-seismic recovery of dislocations in SWUE and KBBRs would allow for a longer time span since diffusion should be considered sluggish at the estimated environmental conditions of ~350°C (Bestmann et al., 2021). Given that kink bands are more severely deformed and the initial sharp CL signal of the lamellae (as seen in the host) is blurred we conclude that the lower CL intensity along the lamellae developed before kinking has started.

Based on misorientation axis information none of the commonly identified slip system can be deduced for the SWUE oriented subparallel to one of the rhombohedral planes {*10-11*}. Assuming a single type of edge dislocations and tilt boundaries, the strong cluster of misorientation axis around *c* would point to *{m}<a>* slip (Neumann, 2000). However, then the misorientation axis should plot within the LABs, which is not the case. Assuming a pure twist boundary (with a minimum of 2 types of dislocation required) the misorientation axis should be perpendicular to the LABs (Lloyd, 2004), which is again not the case. Therefore, the 40-60° angle between misorientation axis and the LABs (Fig. 5h) suggests the existence of a combination of edge and screw dislocations. The SWUE could be produced by recovery of dislocations piled up on rhombohedral slip bands. The WBVs plot around one of the *m*-poles (Fig. 5d-IV) but {*m*} is not a verified Burgers vector in quartz (Morales et al., 2013). However, if slip was equally partitioned along e.g. $+a_1$ and $-a_3$, *m* would be the weighted average of those two Burgers vectors.

6.2.2 Kinking in quartz

Clustering of misorientation axes around {*z*}/{π'} within KBBRs (0-10° angle between misorientation axis and the KBBR trace, Fig. 5h) is compatible with tilt boundaries formed by {*r*}<*a*> and/or {π}<*a*> edge dislocation (Neumann, 2000). LABs are generally curved and, therefore, the boundary character needs to vary between tilt and twist boundaries. This might explain, why the WBVs scatter between

<*a*> and {*m*} (Fig. 5e-IV, 5f-IV). Potentially this could result from a combination of e.g. [$+a_1$] and [$-a_3$] slip with different magnitudes, related to the geometry of the LABs (trace). For KBBRs a certain rotation axis (around pole to {*z*}/{π'}) is located within the slip plane (based on the trace of the SWUE CL-features in the kink domain, Fig. 5e-VI+VII, 5f-VI+VII) and is perpendicular to the corresponding slip direction, therefore subparallel to the Y-direction (coinciding with the inferred kinematic vorticity axis) (Figs. 4c-II) (Chen et al., 2021). This means that the crystal rotation axis (plotted in PF_c) is oriented perpendicular to the loading direction (Hagihara and Miyoshi, 2022). In general, kink bands only form if the rotation of the kink band results in a progressive increase of the Schmid factor (Flewitt and Crocker, 1976; Chen et al., 2021). We analysed the generalised Schmid factor for {*r*}<*a*> and {π}<*a*> slip for different orientations of a triaxial deviatoric stress tensor for a possible range of principal stress directions within the kinematic section (SOM-Fig. 4). In general, kink bands tend to develop when the mechanical anisotropy is aligned (sub)parallel to the compressive principal stress direction (Zhang et al. 2022 and references within). Gay and Weiss (1974) demonstrated experimentally on foliated rocks that the angle α between the principal stress direction and the planar anisotropy controls whether a set of conjugate kinks (α 0-5°) or a single set of kinks (α 5-15°) develop. Therefore, we assume an angle α of 5-13° to be in accordance with the characteristic single kink orientation in combination with the inclination geometry (angle β) of the KBBRs with respect to the general sense of shear (dextral) (and shear zone, Bestmann et al., 2021) as well as to be able to activate slip of the (*r*)[*a*] slip system with the burgers vector within the kinematic section (SOM-Fig. 4). Nishikawa and Takeshita (1999) showed for quartz veins deformed under sub-greenschist conditions that quartz grains unfavourably oriented for easy-slip on the basal plane (hard orientation) exhibit kinking that, in contrast, is not present in grains in a soft orientation. The kinked quartz grains show abundant sub-basal deformation lamellae oriented (sub)parallel to the maximum compressive stress. Based on the elastic multilayer model of Honea and Johnson (1976), Nishikawa and Takeshita (1999) showed by numerical modelling that the kink band width changes as a function of the angle between the sub-basal deformation lamellae and the orientation of maximum

compressive stress. The width of kink bands is narrower when the inferred shortening direction is (sub)parallel (α 0-10°) (Carter et al., 1964) and corresponds to the findings of the Schober quartz microstructures. In lamellar alloys with a harder and softer phase, kink bands develop when only one slip system is predominantly operative (Hess and Barrett, 1949; Hagihara and Miyoshi, 2022). The harder phase prevents that shear cut across the lamellar interface and favours strain localization parallel to mechanic anisotropy (Hagihara and Miyoshi, 2022). For quartz, we interpret that the deformation lamellae with high dislocation density represent the harder lamellar domain that prevents homogeneous distribution of strain within the crystal.

6.3 Evolution model of kinking in quartz during the seismic cycle

First, we consider the regional stress trajectory field related to the geometry of the seismic fault zone and the sample fabric. Then, we discuss a model for the evolution of quartz kinking with respect to the seismic cycle.

6.3.1 Kinking of quartz in a transtensional stress regime

The investigated quartz vein sample is close to a E-W striking pseudotachylyte-bearing dextral strike-slip fault, likely associated with the Oligocene-Miocene transpressional fault system accommodating shortening and the lateral escape of the Alpine stack at the front of the Dolomites indenter (Ratschbacher et al., 1989; Bestmann et al., 2021). However, the direction of σ_1 to the vein-parallel (horizontal) SWUE and the orientation of KBBRs together with the dextral shear sense suggest that the quartz kink bands developed in a transtensional regime (SOM-Fig. 4f) (Grasemann et al., 2019). Transtensional shearing in an overall transpressional regime can be explained by the location of the sample close to the slip plane in the compressional quadrant of a strike-slip fault (Pollard and Segall, 1987). Here, the displacement component perpendicular to the fault is directed away from the fault

resulting in a diverging displacement perturbation field with a local transtensional deformation (compare fig. 2b and 3 in Grasemann et al., 2005).

6.3.2 Pre-seismic loading or seismic rupture propagation: differential stress-induced deformation lamellae (Fig. 8-I)

The fact that the densely spaced deformation lamellae in the deformed quartz veins occur only in the vicinity to a pseudotachylyte bearing fault zone suggest that their formation is related to seismic events. Deformation lamellae in quartz indicate high differential stresses in the range of 170-420 MPa (Drury and Humphrey, 1988; Blenkinsop and Drury, 1988; Drury 1993). Therefore, they can develop during the loading stage preceding the earthquake. In general, deformation lamellae in nature and experiments originate in planes of high shear stress (Carter et al., 1964) and are mainly oriented sub-parallel to the basal plane or to prism planes in some cases (White, 1973; Drury, 1993). Veronique and Langenhorst (2005) showed in deformation experiments that deformation lamellae also develop subparallel to rhombohedral planes especially if the grain is oriented in a hard orientation with respect to the principal stress direction, at differential stress of around 400 MPa. Even higher transient differential stresses (in the range of GPa, Toffol et al., 2024) can be associated with coseismic rupture propagation and may have caused the extremely high density of deformation lamellae in all grains of the sample independent of their crystallographic orientation (SOM-Fig. 1). However, the resetting towards low CL intensity along the deformation lamellae has to occur in a very narrow time window before the kinking process started (see *section 6.2.1 and 6.3.3*). Bestmann et al. (2012, 2016) showed that the resetting of the CL signal of seismically induced fractured quartzite, preserved as CL microstructure in the host rock next to a pseudotachylyte vein and incorporated within the pseudotachylyte, occurred in the timespan between the rupture tip propagation and fault slip event. Therefore, a change of the CL signal in quartz towards lower

intensity (Ti^{4+} reduction most likely triggered by fluids, Bestmann et al., 2021) can happen very fast and might be related to seismic events.

Independent of the timing of the development of deformation lamellae, the question arises whether the dynamic recovery of the initial high dislocation density within the deformation lamellae, resulting in LABs which now define the SWUE, occurred before or after the kink process. A high dislocation density within the deformation lamellae hampers the out-of plane movement of kinking-related dislocations (Zhang et al., 2022) and therefore favours that predominantly dislocations with a glide plane parallel to the lamellar structure of the grain are glissile and able to traverse over longer distances. Hence, we suggest that recovery was post-kinematic to kinking since dynamic recovery before kinking would have reduced the mechanical anisotropy across the deformation lamellae.

6.3.3 Coseismic slip: initiation of kinking by fast athermal dislocation glide (Fig. 8-II)

Kinking in quartz should be roughly coeval to the kinking in mica since otherwise differentially strained/shortened layers would result in a geometric space problem. In other words, there would be a need to store the differential displacement when mica kinks first and quartz kinks at some point later, e.g. during post-seismic deformation under residual stress. We propose that slip of dislocations generated during the coseismic deformation is controlled by the pre-existing crystallographic orientation of the deformation lamellae and its geometry with respect to the stress field. Only the dislocations with the glide planes parallel to the deformation lamellae (one *r*-plane) and the burgers vector within the kinematic section were able to glide, pile up and cause buckling initiation (Hagihara and Miyoshi, 2022), roughly at the same stage when mica kinking occurred during the coseismic event. The slip system {*r*}<*a*> has a high energy factor and is not the most favourable one (Heinisch et al., 1975). However, {*r*}<*a*> is the only slip system allowing dislocations to move over large distances between the deformation lamellae and can be activated at the high differential stresses of coseismic deformation. Other slip systems, with higher Schmid factor and better energy factor, likely became

inefficient after a short gliding distance by abutting against the deformation lamellae. In fact, deformation lamellae with the initially high dislocation density acted as barriers for those systems non-parallel to the lamellae (Hagihara and Miyoshi, 2022).

The question arises of how dislocations could move fast enough in order to initiate kinking during the coseismic event, at the ambient conditions of 300-350 °C (Bestmann et al., 2021). Bestmann et al. (2012) described transient high temperature during coseismic deformation adjacent (1-2 mm) to a pseudotachylyte fault vein. This is not the case for the Schober quartz vein that is too distant (1-1.5 m) from the fault to be affected by the thermal anomaly associated with seismic slip. Initial fast dislocation movement can be explained by the athermal dislocation glide model. Due to the high transient stress state during the coseismic event the Peierls stress of quartz with its relative strong chemical bonds can be easily overstepped and the fast motion of defects is possible without the help of thermal activation (Karato, 2008).

We envisage the following model of kinking development. Kinking initiated from piling up of dislocation after a specific slip distance parallel to the deformation lamellae dislocations. Further addition of dislocations into the pile up caused progressive elastic buckling of the crystal lattice and, in turn, an increase of the Schmid factor of {*r*}<*a*> slip parallel to the deformation lamellae (SOM-Fig. 4e). Even if the Schmid factor did not play a major role for the activation of slip systems, the presumption is that the Schmid factor for the active slip systems which accommodated kinking parallel to the deformation lamellae did increase during the continuous orientation change in the kink domain, and therefore acted as a self-enhanced process (Takagi et al., 2019; Chen et al., 2021). The local differential stress drives dislocations with one sign (black, Fig. 8) to glide toward the upper KBBR (even when not sharply developed at this state) and dislocations of the opposite sign (grey, Fig. 8) to glide toward the lower KBBR (WBV PF_s plots, Fig. 5e-V, 5f-V). This is in accordance with the finding of Burgers (1939) that during kinking sub-parallel arrays of edge dislocations move in

opposite direction and concentrate in pairs along a series of parallel slip planes (Orowan, 1942; Frank and Stroh, 1952). Within all analysed kink domains, a reversed sinistral sense of shear (with respect to general dextral sense of shear of the sample) is required/observed to accommodate the strain and is in accordance with the geometric evolution of kink band structures observed from crystal plastic experiments in metals (Hagihara and Miyoshi, 2022; Zhang et al., 2022). Progressive accumulation of dislocations results in deformation bands which increase the final misorientation between host domain and kink domain (Carter et al., 1964; Hagihara and Miyoshi, 2022). Note, no LABs developed during that stage, since climb is comparably slow with respect to the high strain rate. Roberts and Gow (1958) concluded, from deformation experiments on aluminium, that deformation bands are more abundant at lower temperatures and/or faster strain rate. Carter et al. (1964) came essentially to the same conclusions. They observed in quartz deformation experiments plenty of repetitive deformation and kink bands (in combination with deformation lamellae) at the experimental strain rate and explained that "the paucity of kink band in naturally deformed quartz may be attributable to the slower strain rates in natural deformation". Since the transient strain rate was very high compared to "normal" geological strain rates, this explains why we observe in the Schober quartz vein such high densities of kink bands,

At some point (quite initially) slip systems at high angles relative to the deformation lamellae have to accommodate the geometrically necessary thickening of the kink domains during progressive kinking to prevent openings (see also videos in the supplementary material of Zhang et al., 2022). This could be related to the activity of one of the slip systems with a higher Schmid factor (not necessarily {*r*}<*a*>), which are not parallel to deformation lamellae (SOM-Fig. 4d). As a result, the layer between the deformation lamellae broadens and subsequently the former sharp CL signal is blurred (Fig. 2c).

In lamellar materials kinking starts with buckling (Jelf and Fleck, 1992) and a stable geometry is established already after small strain (Gay and Weiss, 1974; Zhang et al. 2022). There is a strict lock-up condition at $\Psi = 2\beta$ (Nizolek et al., 2021) where Ψ is the tilt angle of the kink domain with

respect to the host domain and β the inclination angle of the KBBR with respect to the vertical axis (Fig. 3). Since the angles β and Ψ are in a relatively small range (Fig. 3), we conclude that after the initial kink process (buckling by development of deformation bands) the geometry was relatively stable. We assume that kink bands did not grow laterally by kink band migration of the KBBRs through the host material as proposed by models of Twiss and Moores (1992). This would require that the entire KBBRs, containing now subparallel LABs, migrated together through the crystal, which seems very unlikely. Further in this model the angle φ and φ_k remains equal which is not the case for this study.

6.3.4 Post-seismic creep: dynamic recovery (Fig. 8-III)

We postulate that, after initial kinking, dynamic recovery occurred during post-seismic deformation under residual stress, which is a general phenomenon in seismogenic zones following an earthquake (Trepmann and Stöckhert, 2013). The accumulated dislocations reorganized into SGBs since under the lower post-seismic strain rates dislocation were able to climb at the ambient condition of 300-350 °C. Similar to the experiments of Zhang et al. (2022) several (sub)parallel SGBs (1.5-4.5°) accommodated the large rotation angle (33-43°) across the KBBRs. Therefore, the arrangement of subparallel SGBs, which now characterise the KBBRs (width 10-30 µm), reflects the initial KBBRs (deformation bands) with the highest misorientation across. SGBs can coalescence to form new (sub)grain boundaries or even iHAGB (10-20°/25°) especially evident where the KBBR width is < 10 µm (compare fig. $8b_4$ in Zhang et al., 2022). Note, all (sub)grain boundaries within KBBRs show a cluster of misorientation axis around{*z*}/{π'}, also iHAGB (Fig. 4c-II), indicating dominant {*r*}<a> and, to a minor degree, {π}<*a*> slip (based on Schmid factor analyses, SOM-Fig. 4). Within kink domains, SGBs (1.5-4.5°) developed (sub)parallel to KBBRs due to dynamic recovery of dislocations on one of the *r*-planes parallel to the initial deformation lamellae. As a result, the former internal structure of the deformation lamellae is overprinted and only visible as relicts within the CL images. During the

initial layer-parallel slip or during post-seismic creep the fluid inclusion were erased within the kink domain. Outside of the kink domains, dynamic recovery modifies the former deformation lamellae into SWUE, with a low(er) dislocation density (Vernooij and Langenhorst, 2005; Trepmann and Stöckhert, 2013).

Since kinking can only accommodate limited strain (Gay and Weiss, 1974; Nizolek et al., 2020), further quartz deformation was accomplished by activation of intra- and inter-crystalline microshear zones (sub)parallel to the fault zone (SOM-Fig. 2). Paleostress piezometry based on the quartz (sub)grain size of 3-5 µm (mean equivalent diameter) and of 3.4 µm (root mean square grain size), developed by subgrain rotation recrystallization yields flow stresses of 160-210 MPa and 200 MPa, respectively, for this stage of deformation (Stipp and Tullis, 2003; Cross et al., 2017) (SOM-Fig. 2). These relatively high differential stresses are interpreted to reflect the localized strain rates during the immediate stages of stress relaxation following the main earthquake event.

7. Conclusion

Quartz kinking in a quartz vein next to a pseudotachylyte-bearing fault zone in the Schobergruppe (Austroalpine Crystalline Complex, Eastern Alps) was promoted by formation of deformation lamellae at transient high differential stresses during the seismic event, either during the loading stages preceding the earthquake or during the seismic rupture propagation. Deformation lamellae with an initial high dislocation density acted as barriers for dislocation movement during high strain rates. Only dislocations parallel to the deformation lamellae (*r*-planes) were able to glide over significant distances. The other slip systems, with different slip directions (even when easier to activate), were blocked after a short gliding distance abutting against the deformation lamellae. We suggest that athermal dislocations glided fast, piled up and caused kink initiation during the coseismic event. Quartz kinking occurred during the same seismic event inducing kinking of micas in the vein host rock. During post-seismic creep at lower residual stress, the accumulated dislocations in deformation

bands (initial kink band boundary regions) reorganized into subparallel subgrain boundaries at the ambient condition of 300-350 °C. Paleopiezometer analysis of kink-related microshear zones revealed that the post seismic creep took place at around 200 MPa. Therefore, intensive kinking of quartz and mica is an important process of strain accommodation in crystals during coseismic high differential stress, and can be used as indicators of paleoseismicity.

CRediT authorship contribution statement

Michel Bestmann: Funding acquisition, Investigation, Conceptualization, Formal analysis, Validation, Data curation, Visualization, Supervision, Writing – original draft, review and editing. **Bernhard Grasemann:** Funding acquisition, Writing – review & editing, Validation, Formal analysis, Investigation. **Rüdiger Kilian:** Formal analysis, Validation, Visualization, Software, Writing – review & editing**. John Wheeler:** Writing – review & editing, Validation, Software. **Luiz F.G. Morales:** Formal analysis. **Andreas Bezold:** Formal analysis, Writing – review & editing. **Giorgio Pennacchioni:** Funding acquisition, Writing – review & editing, Validation.

Acknowledgments

This work was supported by the Deutsche Forschungsgemeinschaft DFG (BE2413/3-1) and the FWF Austrian Science Fund (Project POLARIS, I 5399-N). GP acknowledges funding from PRIN_2020WPMF39 (project: THALES). We acknowledge Holger Stünitz for providing access to the SEM-CL spectra facilities at the Department of Geosciences at the Arctic University of Norway (Tromsö), and Tom-Ivar Eilertsen for his assistance. Access to the SEM-EBSD and TEM facilities was provided by the Department of Materials Science and Engineering WW1, FAU Erlangen-Nürnberg, Germany. The Oxford Instruments CMOS-Symmetry EBSD detector was funded by the DFG (JA 2718/3-1).

Figure captions

Figure 1. (a) Simplified geological map of part of the Eastern Alps (modified after Schuster et al., 2014). Important Tertiary fault systems are given. Note sampled fault (red stippled line) is a continuation in strike of the Defereggental-Anterselva-Valles fault (DAV). Innsbruck-Salzburg-Amstetten fault (ISAM); Salzach-Ennstal-Mariazell-Puchberger fault (SEMP); Mur-Murztal fault (MM); Lavanttal fault (LA); Molltal fault (MO); Iseltal fault (IS). (b) Field pictures of layer-parallel quartz veins with respect to the foliation of the host rock paragneiss. (c) Sample location of the analysed quartz vein (HS-2017-4) and the adjacent host rock paragneiss (HS-2017-4b) (UTM33 326574 E/ 5198989 N), ca. 1.5-2 m distance to the seismic fault zone. (d) Pseudotachylyte (UTM33 326542 E/ 5198982 N) from the fault zone.

Figure 2. (a) Quartz vein with intensively kinked quartz grains (optical microphotograph under crossed polarized light, XPL). (b) Area as marked in (a). (c) Corresponding cathodoluminescence images, CL, to optical image (b) reveal intense laminar structures across kinked quartz grains. Note, areas with narrow and sharply developed horizontal lamellae are the host domains and areas with inclined and blurred/broader lamellae represent kink domains.

Figure 3. Sketch of quartz kind band microstructure and geometry parameters. General sense of shear is dextral. Note, weighted Burgers vectors (WBV) plot in opposite directions for the corresponding kink band boundary regions (KBBRs).

Figure 4. Electron backscatter diffraction, EBSD, data of kinked quartz microstructures as shown in Fig. 2b. (a, b) EBSD orientation map, colour coded with respect to the Z-direction (sample reference system) (step size 250 nm, boundary levels are given). (c) Orientation data of map presented in (b). (I, II, III) Data of different microstructural domains across kinked area. Crystallographic axes and planes

are presented as pole figure (upper row), PF (lower hemisphere), and misorientation axes of low angle boundaries (<10°) as inverse pole figures, IPF_c (crystallographic coordinates), and as PF_s (sample coordinates) for different misorientation angle intervals (lower rows). Blue circle marks centre of the cluster of misorientation axis for the horizontal lamellae (short-wavelength undulatory extinction, SWUE) in the host domain and orange circle for the kink band boundary regions (KBBR). In (II) IPF_c indicating theoretical slip systems in quartz, assuming edge dislocations, for specific misorientation axis (after Neumann, 2000). The clustering between π`and *z* corresponds to slip systems *r<a>* and/or π*<a>*.

Figure 5. Detailed EBSD data analysis across kink microstructure. (a) CL image. (b) Backscatter electron orientation contrast (BSE-OC) image. Note, porosity along horizontal lamellae (white arrows and magnified inset). (c) EBSD orientation map of same microstructures as presented in (a) and (b). (d-f) EBSD data of horizontal lamellae (SWUE), kink band boundary regions $KBBR_A$ and $KBBR_B$. (I) EBSD orientation maps. Coloured lines represent subgrain boundaries <10° and blue lines high angle boundaries >10-15° following Fig. 4b. (II, III) Map with Weighted Burges Vectors (WBV). (IV, V) WBV plotted in crystallographic coordinates, IPF_c, and in sample coordinates, PF_s (all data plotted + contoured). Note in (V), for the two kink band boundary regions $KBBR_A$ and $KBBR_B$ the WBV point to different directions. (VI) Orientation data plotted in PF_s (lower hemisphere). Trace/dip of SWUE and KBBRs are marked with different coloured lines and the specific misorientation axes are indicated by coloured circles. (VII) Misorientation axis of low angle boundaries (1-10°) are plotted in crystallographic coordinates, IPF_c, and in sample coordinates, PF_s. (g) Misorientation profile across kink band boundary region. (I) EBSD orientation map colour coded with respect to orientation spread (see colour code). (II) Misorientation angle along line, as given in (I), relative to point A. (III) Misorientation angle from point to point. Note, sub(parallel) subgrain boundaries accumulate total misorientation angle of 38° across kink band boundary with a transition width of ca. 20-25 µm. (h) Boundary map shows the angle of misorientation axis with respect to the trace of subgrain

boundaries – see colour code, which can be used to indicate tilt boundaries versa twist boundaries and mixed boundary configuration.

Figure 6. TEM analysis across (a) horizontal lamellae (SWUE) and (b) kink band boundary region. Both TEM lamellae were cut perpendicular to map surface. (I) EBSD orientation map with location of FIB lamella (boundary levels follow Fig. 4b). (II) Misorientation profile along trace of FIB lamella. Misorientation angle of low angle boundaries (LABs) are given. (III) TEM mosaic (bright field images) of FIB lamella. LAB-2 in (a) and LAB-4 in (b) shows ordered dislocations. In general, the dislocation density is very low, especially across horizontal SWUE. Note, since for all samples beam damage during TEM analysis was very fast, it was only possible to capture one image per area of interest, under the working TEM conditions (with the highest diffraction contrast). Therefore, a quantitative estimate of the dislocation density was not possible and only a comparative density description between the investigated areas is provided.

Figure 7. Kinked micas. (a) Host rock gneiss containing up to 1 mm thick nearly pure mica layer – biotite and muscovite (a-e: optical microphotographs, XPL). (b) Micas in the mica-layer are heavily kinked, but isolated micas in the gneiss matrix rarely. (c, d) Micas can show different kink band boundary orientation. (e) Optical micrograph of kinked mica aggregate analysed by backscatter electrons (BSE). (f) BSE image of same area as in (e) shows a kinked aggregate of biotite (*Bt*), muscovite (*Msc*) and chlorite (*Chl*). (g, h) High magnification BSE images from areas as marked in (f). (g) Primary kinking (Etheridge et al., 1973) in muscovite. (h) Opening gaps in muscovite along cleavage planes induced during the kink process.

Figure 8. Evolution model for the kinked quartz grains modified after Zhang et al. (2022).

References:

Anderson, E.K., Song, W.J., Johnson, S.E., Cruz-Uribe, A.M., 2021. Mica kink-band geometry as an indicator of coseismic dynamic loading. Earth Planet. Sci. Lett. 537, 117000. https://doi.org/10.1016/j.epsl.2021.117000.

Aslin, J., Mariani, E., Dawson, K., Barsoum, M.W., 2019. Ripplocations provide a new mechanism for the deformation of phyllosilicates in the lithosphere. Nat. Commun. 10. https://doi.org/10.1038/s41467-019-08587-2.

Bell, I.A., Wilson, C.J.L., McLaren, A.C., Etheridge, M.A., 1986. Kinks in mica: role of dislocations and (001) cleavage. Tectonophysics 127, 49–65. https://doi.org /10.1016 /0040 -1951(86)90078 -8.

Bestmann, M., Pennacchioni, G., Frank, G., Göken, M., de Wall, H., 2011. Pseudotachylyte in muscovite-bearing quartzite: coseismic friction-induced melting and plastic deformation of quartz. J. Struct. Geol. 33, 169-186.

Bestmann, M., Pennacchioni, G., Grasemann, B., Huet, B., Jones, M.W.M., Kewish, C.M., 2021. Influence of deformation and fluids on Ti exchange in natural quartz. J. Geophys. Res., Solid Earth 126. https://doi.org/10.1029/2021JB022548.

Bestmann, M., Pennacchioni, G., Mostefaoui, S., Göken M., de Wall, H., 2016. Instantaneous sealing of micro-fractures during coseismic slip: evidence from microstructure and Ti in quartz geochemistry within an exhumed pseudotachylyte-bearing fault in tonalite. Lithos 254-255, 84-93.

Bestmann, M., Pennacchioni, S., Nielsen, G., Göken, M., de Wall, H., 2012. Deformation and ultrafine recrystallization of quartz in pseudotachylyte-bearing faults: a matter of a few seconds. J. Struct. Geol., Special Volume: Physico-chemical processes in seismic faults. J. Struct. Geol. 38, 21-38.

Bestmann, M., Prior, D.J., 2003. Intragranular dynamic recrystallization in naturally deformed calcite marble: diffusion accommodated grain boundary sliding as a result of subgrain rotation recrystallization. J. Struct. Geol. 25, 1597-1613.

Blenkinsop, T.G., Drury, M.R., 1988. Stress estimates and fault history from quartz microstructures, J. Struct. Geol. 10, 673–684.

Burgers, J.M., 1939. Some considerations on the field of stress connected with dislocations in a regular crystal lattice. Proceedings of the Koninklijke Nederlandse Akademie van Wetenschappen 42, 293.

Carter, N.L., Christie, J.M., Groggs, D.T., 1964. Experimental deformation and recrystallization of quartz. J. Geol. 72, 687-733.

Chen et al., 2021. Influence of Temperature and Plastic Strain on Deformation Mechanisms and Kink Band Formation in Homogenized HfNbTaTiZr. Crystals 11, 81.

Christie, J.M., Griggs, D.T., Carter, N.L., 1964. Experimental evidence of basal slip in quartz. J Geol. 72, 734-756.Cowan, D.S., 1999. Do faults preserve a record of seismic slip? A field geologist's opinion. J. Struct. Geol. 21, 995–1001. https://doi.org /10 .1016 /S0191 -8141(99)00046 -2.

Cook, D.H., Kumar, P., Payne, M., Belcher, C.H., Borges, P., Wang, W., Walsh, F., Li, Z., Devaraj, A., Zahng, M., Asta, M., Minor, A.M., Lavernia, E.J., Apelian, D., Rutchie, R.O., 2024. Kink bands promote exceptional fracture resistance in a NbTaTiHf refractory medium-entropy alloy. Science 384, 178-184. https://doi .org/0.1126/science.adn2428.

Cowan, D.S., 1999. Do faults preserve a record of seismic slip? A field geologist's opinion. J. Struct. Geol. 21, 995–1001.

Cross, A.J., Prior, D.J., Stipp, M., Kidder, S., 2017. The recrystallized grain size piezometer for quartz: An EBSD-based calibration. Geophys. Res. Lett. 44, 6667–6674. https://doi .org/10.1002/2017GL073836.

Di Toro, G., Nielsen, S., Pennacchioni, G., 2005. Earthquake rupture dynamics frozen in exhumed ancient faults. Nature 436, 1009–1012. doi: 10.1038/nature03910.

Drury, M.R., 1993. Deformation lamellae in metals and minerals. In: Boland, J.N., Fitz Gerald, J.D. (Eds.), Defect and Processes in the Solid State: Geoscience Application. Elsevier, Amsterdam, pp. 195–212.

Drury, M.R., Humphreys, F.J., 1988. Microstructural shear criteria associated with grain boundary sliding during ductile deformation. J. Struc. Geol. 10, 83-99.

Drury, M.R., Urai, J.L., 1990. Deformation-related recrystallization processes. Tectonophysics 172, 235–253.

Durinck, J., Devincre, B., Kubin, L., Cordier, P., 2007. Modelling the plastic deformation of olivine by dislocation dynamics simulations. Am. Mineral. 92, 1346–1357.

Ebert, M., Poelchau, M.H., Kenkmann, T., Gulick, S.P.S., Hall, B., Lofi, J., McCall, N., and Rae, A.S.P., 2021, Comparison of stress orientation indicators in Chicxulub's peak ring: Kinked biotites, basal PDFs, and feather features, *in* Reimold, W.U., and Koeberl, C., eds., Large Meteorite Impacts and Planetary Evolution VI: Geological Society of America Special Paper 550, p. 479–493. https://doi.org/10.1130/2021.2550(21).

Etheridge, M.A., Hobbs, B.E., Paterson, M.S., 1973. Experimental deformation of single crystals of biotite. Contrib. Mineral. Petrol. 38, 21–36. https://doi .org /10 .1007 /BF00371724.

Flewitt, P.E.J., Crocker, A.G., 1976. The Formation of Deformation Kinks in Body Centred Cubic Crystals. Philos. Mag. 34, 877–891.

Frank, F.C., Stroh, A.N., 1952. On the theory of kinking. Proc. Phys. Soc. 65, 811–821.

Gay, N.C., Weiss, L.E., 1974. The relationship between principal stress directions and the geometry of kinks in foliated rocks. Tectonophysics 21, 287–300. https:// doi .org /10 .1016 /0040 -1951(74)90056 -0.

Grasemann, B., Dabrowski, M., Schöpfer, M.P.J., 2019. Sense and non-sense of shear reloaded. Journal of Structural Geology 125, 20-28. https://doi.org/10.1016/j.jsg.2018.05.028.

Grasemann, B., Martel, S., Passchier, C., 2005. Reverse and normal drag along a fault. J. Struct. Geol. 27, 999-1010.

Hagihara, K., Miyoshi, K., 2022. Kink-band formation in directionally solidified Mg/Mg2Yb and Mg/Mg2Ca eutectic alloys with Mg/Laves-phase lamellar microstructure. Journal of Magnesium and Alloys 10, 492-500. https://doi.org/10.1016/j.jma.2021.02.006.

Hamers, M.F., Drury, M.R., 2011. Scanning electron microscope-cathodoluminescence (SEM-CL) imaging of planar deformation features and tectonic deformation lamellae in quartz. Meteorit. Planet. Sci. 46, 1814–1831. doi: 10.1111/j.1945-5100.2011.01295.x

Hauke, M., Froitzheim, N., Nagel, T.J., Miladinova, I., Fassmer, K., Fonseca, R. O. C., Sprung, P., Münker, C., 2019. Two high-pressure metamorphic events, Variscan and Alpine, dated by Lu–Hf in an eclogite complex of the Austroalpine nappes (Schobergruppe, Austria). Int Earth Sci (Geol Rundsch) 108, 1317-1331. https://doi.org/10.1007/s00531-019-01708-8.

Hess, J.B., Barrett, C.S., 1949. Structure and nature of kink bands in zinc. Metal Transaction 185, 599-606.

Heinisch, H.L., Sines, Jr.G., Goodman, W., Kirby, S.H., 1975. Elastic stress and self-energies of dislocations of arbitrary orientation in anisotropic media: olivine, orthopyroxene, calcite and quartz. J. Geophys. Res. 80, 1886-1896.

Honea, E., Johnson, A.M., 1976. A theory of concentric, kink and sinusoidal folding and of monoclinal flexuring of compressible, elastic multilayers: IV. Development of sinusoidal and kink folds in multilayers confined by rigid boundaries. Tectonophysics 30, 197–239. https://doi .org /10 .1016 /0040 -1951(76)90187 -6.

Humphreys, F.J., Hatherly, M., Rollett, A., 2017. Recrystallization and Related Annealing Phenomena, third. ed. Elsevier Ltd.

Karato, S.-I., 2008. Deformation of earth materials: An introduction into the rheology of solid earth. Cambridge University press.

Jelf, P.M., Fleck, N.A., 1992. Compression failure mechanism in unidirectional composites. J. Compos. Mater. 26, 2706-20726.

Linner, M., 1999. Die P-T-t Entwicklung der Eklogite im Schoberkristallin als Beleg für frühalpidische kontinentale Subduktion im Ostalpinen Kristallin. Thesis, University of Vienna, 211 p.

Lloyd, G.E., 2004. Microstructural evolution in a mylonitic quartz simple shear zone: the significant roles of dauphine twinning and misorientation. Geological Society, London, Special Publications 224, 39-61. doi:10.1144/GSL.SP.2004.224.01.04.

Mancktelow, N.S., Camacho, A., Pennacchioni, G., 2022. Time-Lapse Record of an Earthquake in the Dry Felsic Lower Continental Crust Preserved in a Pseudotachylyte-Bearing Fault. J. Geophys. Res., Solid Earth, 127. https://doi.org/10.1029/2021JB022878.

Matsumoto, T., Yamasaki, M., Hagihara, K., Kawamura Y., 2018. Configuration of dislocations in low-angle kink boundaries formed in a single crystalline long-period stacking ordered Mg-Zn-Y alloy. Acta Mater. 151, 112–124. doi: 10.1016/j. actamat.2018.03.034.

McLaren A.C., Turner R.G., Boland J. N., Hobbs B.E., 1970. Dislocation structure of lamellae in synthetic quartz. Contrib. Mineral. Petrol. 29, 104–115.

Menegon, L., Pennacchioni, G., Heilbronner, R., Pittarello, L ., 2008. Evolution of quartz microstructure and c-axis crystallographic preferred orientation within ductilely deformed granitoids (Arolla Unit, Western Alps). J. Struct. Geol. 30, 1332–1347.

Morales, L., Lloyd, G.E., Mainprice, D., 2013. Fabric transitions in quartz via viscoplastic self-consistent modeling part I: Axial compression and simple shear under constant strain. Tectonophysics 636, 52-69. https://doi.org 10.1016/j.tecto.2014.08.011.

Neumann, B., 2000. Texture development of recrystallized quartz polycrystals unravelled by orientation and misorientation characteristics. J. Struct. Geol. 22, 1695–1711.

Nishikawa, O., Takeshita, T., 1999. Dynamic analysis and two types of kink bands in quartz veins deformed under subgreenschist conditions. Tectonophysics 301, 21–34. https://doi.org/10 .1016 /S0040 -1951(98)00219 -4.

Nizolek, T.J., Pollock, T.M. , McMeeking, R.M., 2021. Kink band and shear band localization in anisotropic perfectly plastic solids, J. Mech. Phys. Solids. 146, 104183. https://doi.org/10.1016/j.jmps.2020.104183.

Okubo, K., Bhat, H.S., Rougier, E., Marty, S., Schubnel, A., Lei, Z., Knight, E.E., Klinger, Y. (2019). Dynamics, Radiation, and Overall Energy Budget of Earthquake Rupture With Coseismic Off-Fault Damage. J. Geophys. Res., Solid Earth, 124, 11771–11801. https://doi.org/10.1029/2019JB017304.

Orowan, E., 1942. A type of plastic deformation new in metals. Nature 3788, 643–644.

Piazolo, S., Montagnat, M., Grennerat, F., Moulinec, H., Wheeler, J., 2015. Effect of local stress heterogeneities on dislocation fields: examples from transient creep in polycrystalline ice. Acta Mater. 90, 303–309. https://doi .org/10.1016/j.actamat.2015.02.046.

Pollard, D.D., Segall, P., 1987. Theoretical displacements and stresses near fractures in rocks: with applications to faults, joints, veins, dikes, and solution surfaces. in: Atkinson, B.K. (Ed.), Fracture Mechanics of Rock, Academic Press, San Diego, California, 277-349.

Ratschbacher, L., Frisch, W., Neubauer, F., Schmid, S.M., J. Neugebauer, 1989. Extension in compressional orogenic belts: The eastern Alps. Geology 17, 404-407.

Roberts, J.M., Gow, K.V., 1958. Deformation of single crystals of aluminium, A.I.M.E. Trans 212, 648-658.

Schulz, B., 1993. Mineral chemistry, geothermobarometry and pre-Alpine high-pressure metamorphism of eclogitic amphibolites and mica schists from the Schobergruppe, Austroalpine basement, Eastern Alps. Mineral. Mag. 57, 189-202.

Seidemann, M., Prior, D.J., Golding, N., Durham, W.B., Lilly, K., Vaughan, M.J., 2020. The role of kink boundaries in the deformation and recrystallisation of polycrystalline ice. J. Struct. Geol. 136, 104010. https://doi .org /10 .1016 /j.jsg .2020 .104010.

Short, N.M., 1966. Effects of shock pressures from a nuclear explosion on mechanical and optical properties of granodiorite. J. Geophys. Res. 71, 1195–1215. https://doi .org /10 .1029 /jz071i004p01195.

Schuster, R., Daurer, A., Krenmayr, H.-G., Linner, M., Mandl, G. W., Pestal, G., Reitner, J. M., 2014. Rocky Austria: The Geology of Austria - brief and colourful (pp. 1–80). Geological Survey Austria.

Stipp, M., Tullis, J., 2003. The recrystallized grain size piezometer for quartz. Geophys. Res. Lett. 30, 2088, doi:10.1029/2003GL018444.

Takagi, K., Mayama, T., Mine, Y., Chiu, Y.L, Takashima, K., 2019. Extended ductility due to kink band formation and growth under tensile loading in single crystals of Mg-Zn-Y alloy with 18R-LPSO structure. J. Alloys Compd., 806, 1384-1393. https://doi.org/10.1016/j.jallcom.2019.07.344.

Tarantola, A., Diamond, L.W., Stunitz, H., 2010. Modification of fluid inclusions in quartz by deviatoric stress I: experimentally induced changes in inclusion shapes and microstructures. Contrib. Mineral. Petrol. 160, 825–843.

Trepmann, C.A., Stöckhert, B., 2013. Short-wavelength undulatory extinction in quartz recording coseismic deformation in the middle crust – an experimental study. Solid Earth 4, 263-276.

Toffol, G., Pennacchioni, G., Menegon, L., Wallis, D., Faccenda, M., Camacho, A., Bestmann, M., 2024. On-fault earthquake energy density partitioning from shocked garnet in an exhumed seismic mid-crustal fault. Science advances 10, eadi8533. https://doi.org/ 10.1126/sciadv.adi8533.

Twiss, R.J., Moores, E.M., 1992. Structural Geology. W.H. Freeman and Company, New York, 532.

Vernon, R.H., 2018. A Practical Guide to Rock Microstructure, 2nd ed. Cambridge University Press.

Vernooij, M.G.C., Langenhorst, F., 2005. Experimental reproduction of tectonic deformation lamellae in quartz and comparison to shock-induced planar deformation features. Meteorit Planet Sci 40, 1353–1361.

Wheeler, J., Mariani, E., Piazolo, S., Prior, D.J., Trimby, P., Drury, M.R., 2009. The weighted Burgers vector: a new quantity for constraining dislocation densities and types using Electron Backscatter Diffraction on 2D sections through crystalline materials. J. Microsc. 233, 482–494.

Wheeler, J., Piazolo, S., Prior, D.J., Trimby, P., Tielke, J.A., 2024. Using crystal-lattice distortion data for geological investigations: the weighted Burgers vector method. J. Struct. Geol. 179, 105040. https://doi.org/10.1016/j.jsg.2023.105040.

White, S.H., 1973. Deformation lamellae in naturally deformed quartz. Nat. Phys. 245, 26–28.

White, S.R., 2001. Textural and microstructural evidence for semi-brittle flow in natural fault rocks with varied mica contents. Int J Earth Sciences (Geol Rundsch) 90, 14-27. doi: 10.1007/s005310000166.

Zhang, Y., Li, N., Schneider, M.M., Nizolek, T.J., Capolungo, L., 2022. Kink mechanism in Cu/Nb nanolaminates explored by in situ pillar compression. Acta Materialia 237, 118150. https://doi.org/10.1016/j.actamat.2022.118150

Graphical Abstract

Click here to access/download;Graphical Abstract (for review);GraphicAbstract_Bestmann et al_EPSL_submit_2024-09-09_red.jpg

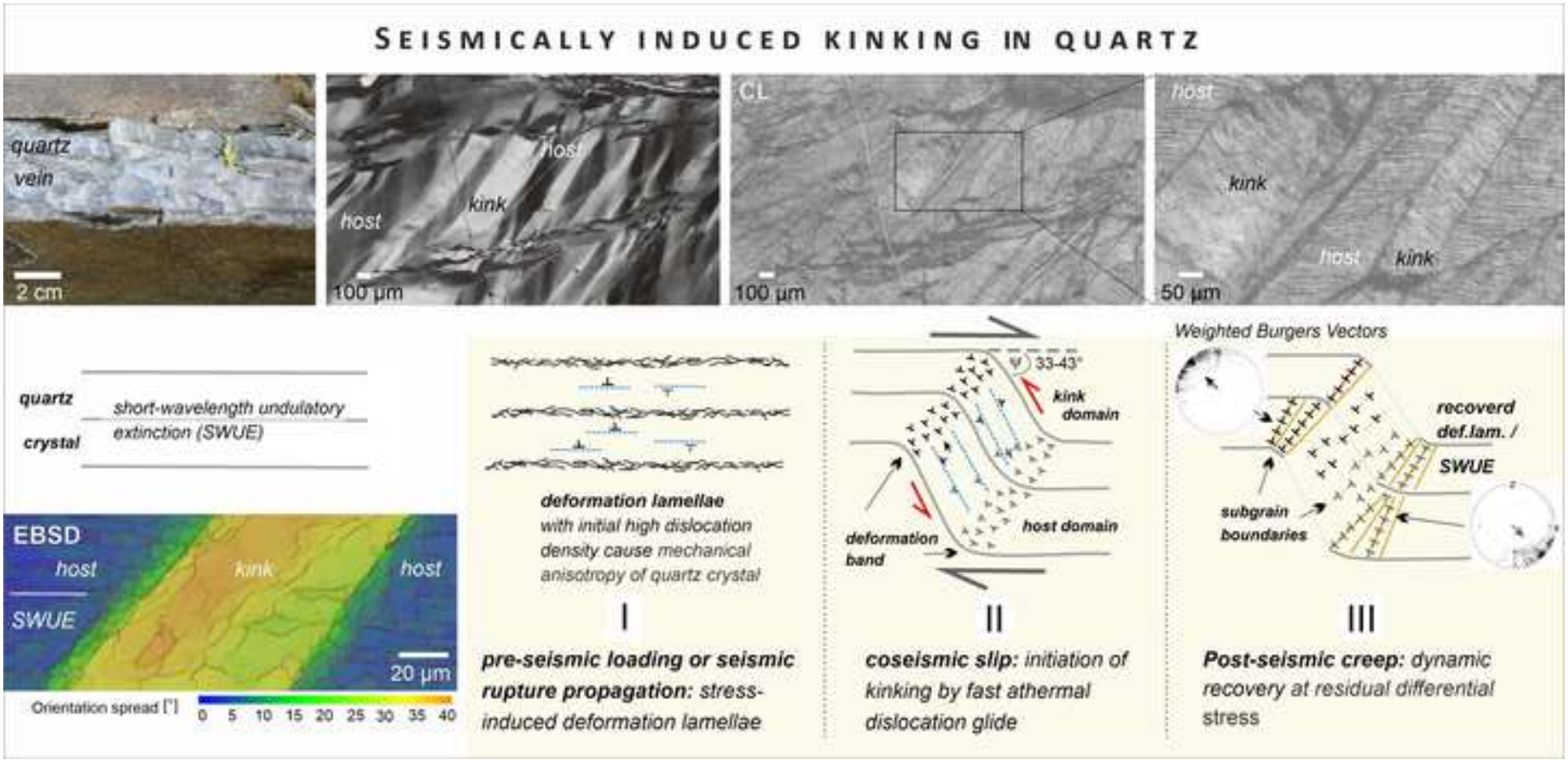

Figure

Click here to access/download;Figure;Fig-1_Bestmann et al_EPSL_submit_location+pst_red.jpg

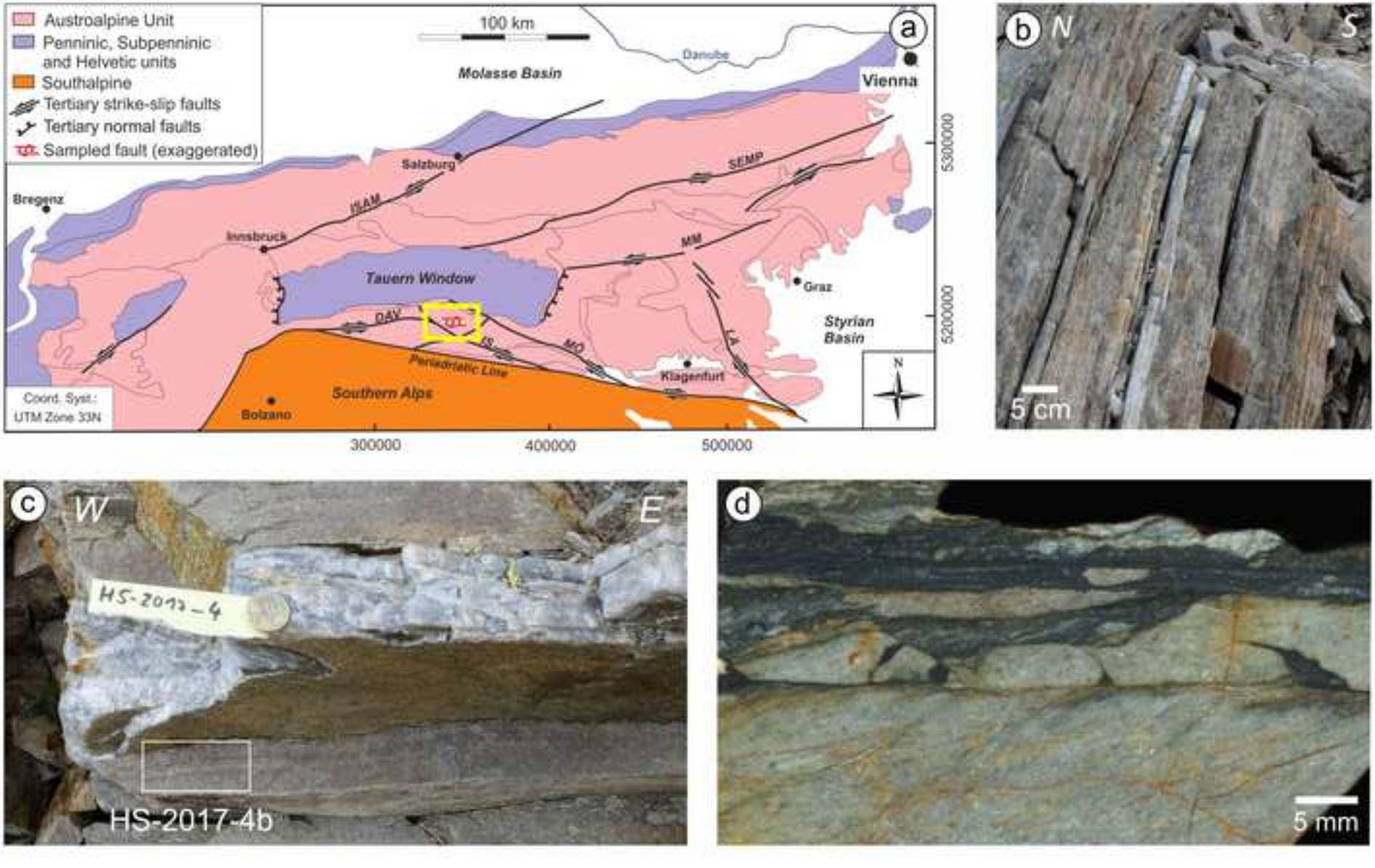

Figure

Click here to access/download;Figure;Fig-2_Bestmann et al_EPSL_submit_qtz-kink_opt+CL_red.jpg

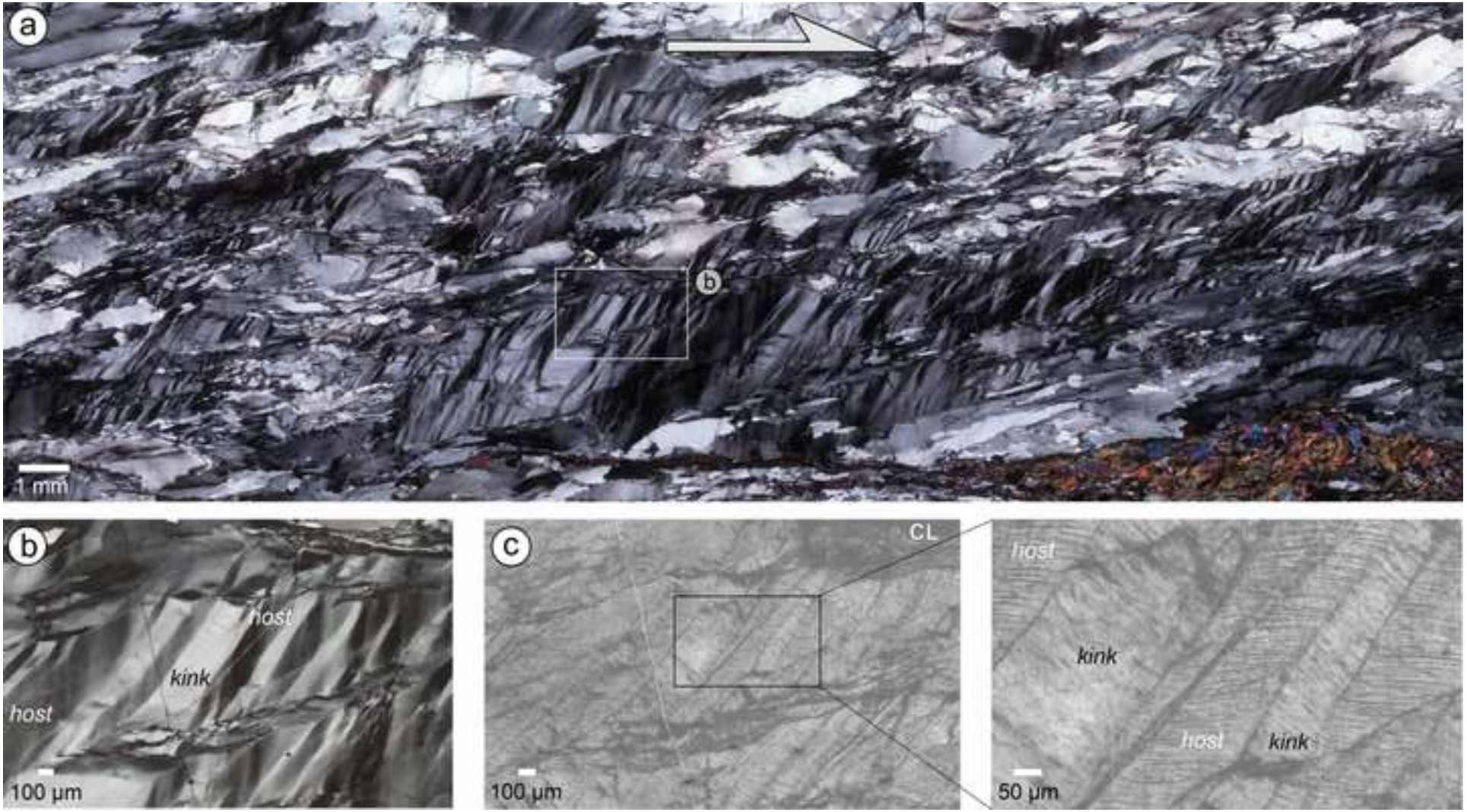

Figure

Click here to access/download;Figure;Fig-3_Bestmann et al_EPSL_submit_qtz-kink_sketch_red.jpg

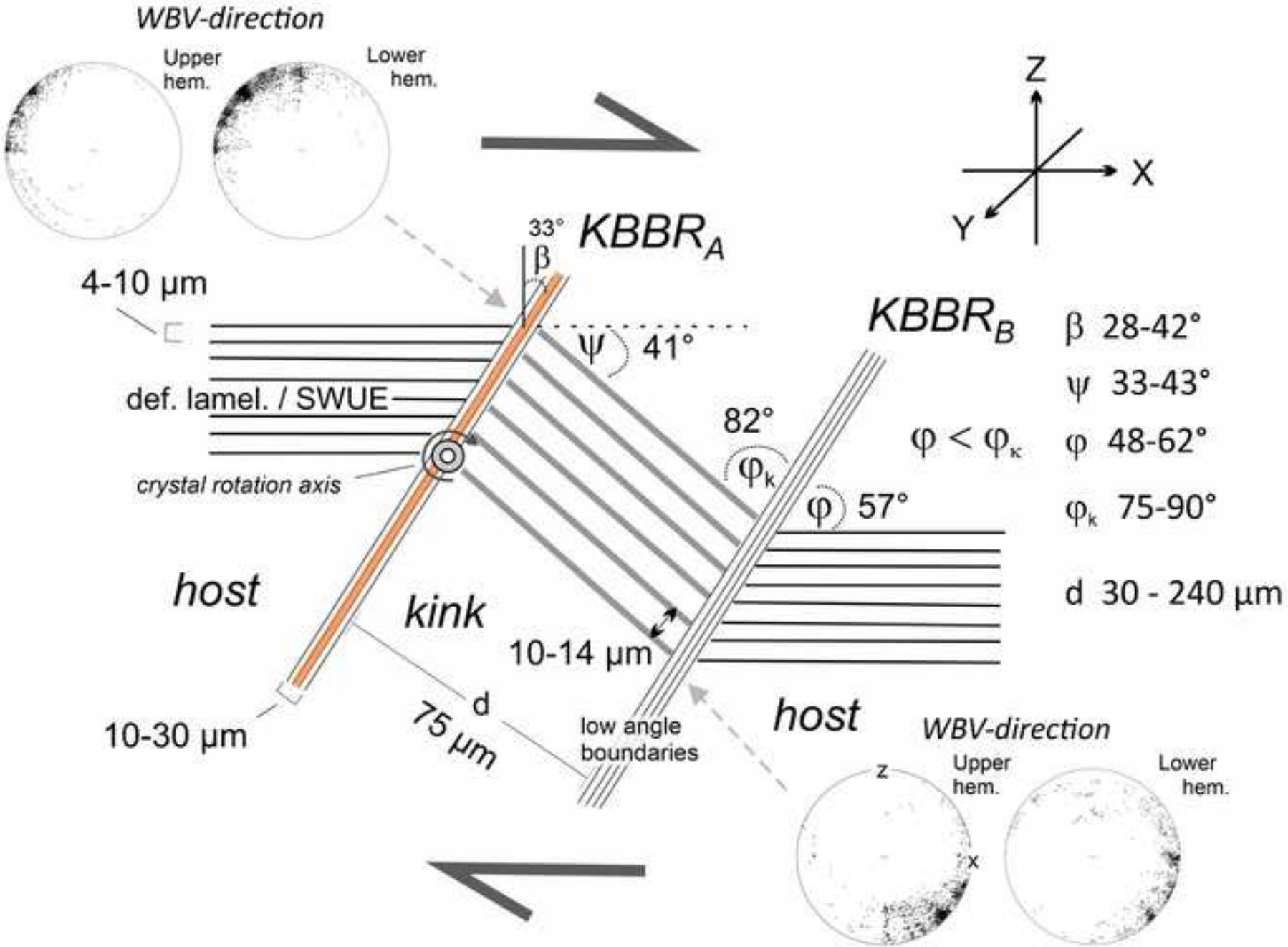

Figure

Click here to access/download;Figure;Fig-4_Bestmann et al_EPSL_submit_qtz-EBSD_red.jpg

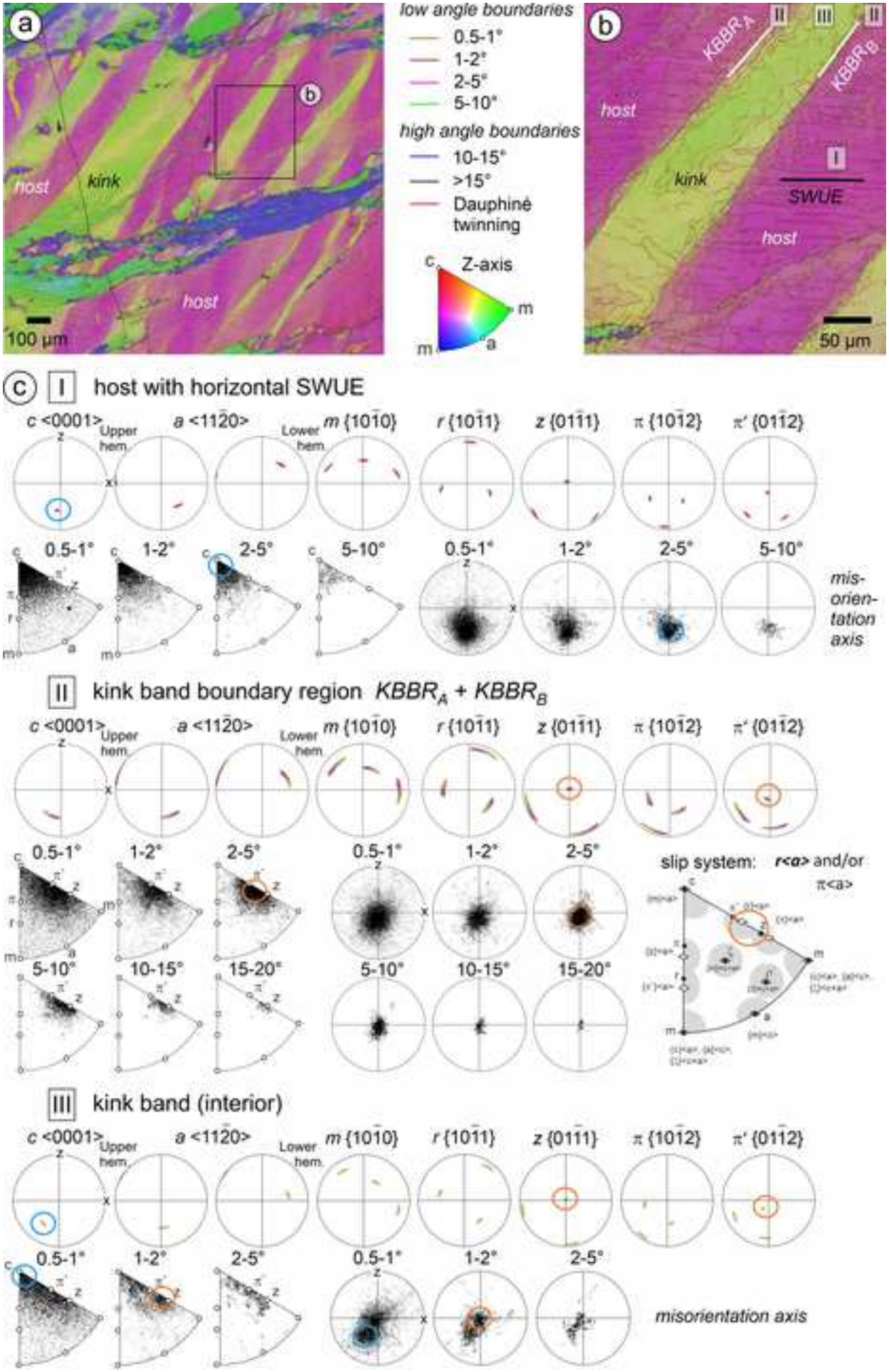

Figure

Click here to access/download;Figure;Fig-5_Bestmann et al_EPSL_submit_EBSDdetail+WBV_red.jpg

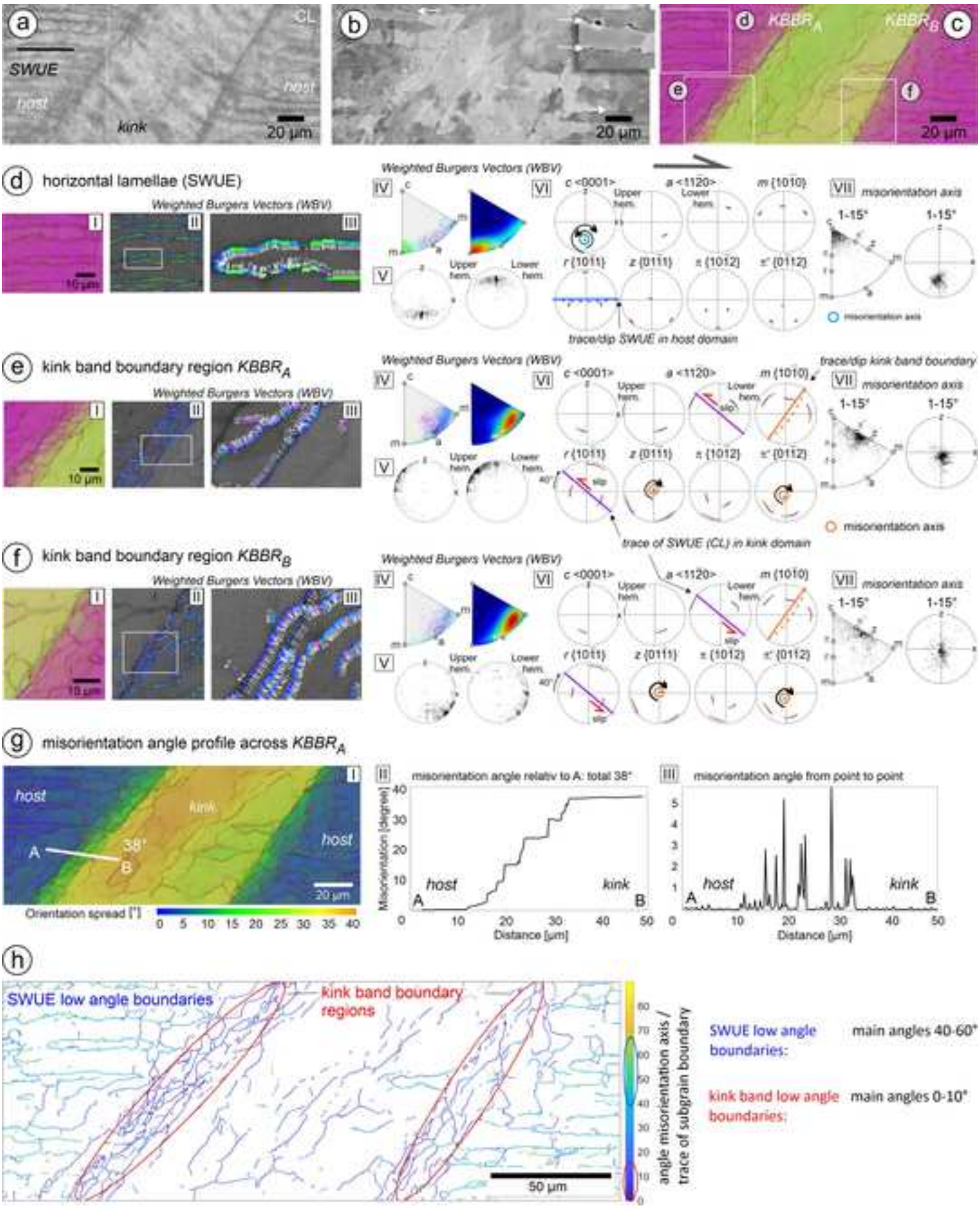

Figure

Click here to access/download;Figure;Fig-6_Bestmann et al_EPSL_submit_FIB+TEM_red.jpg

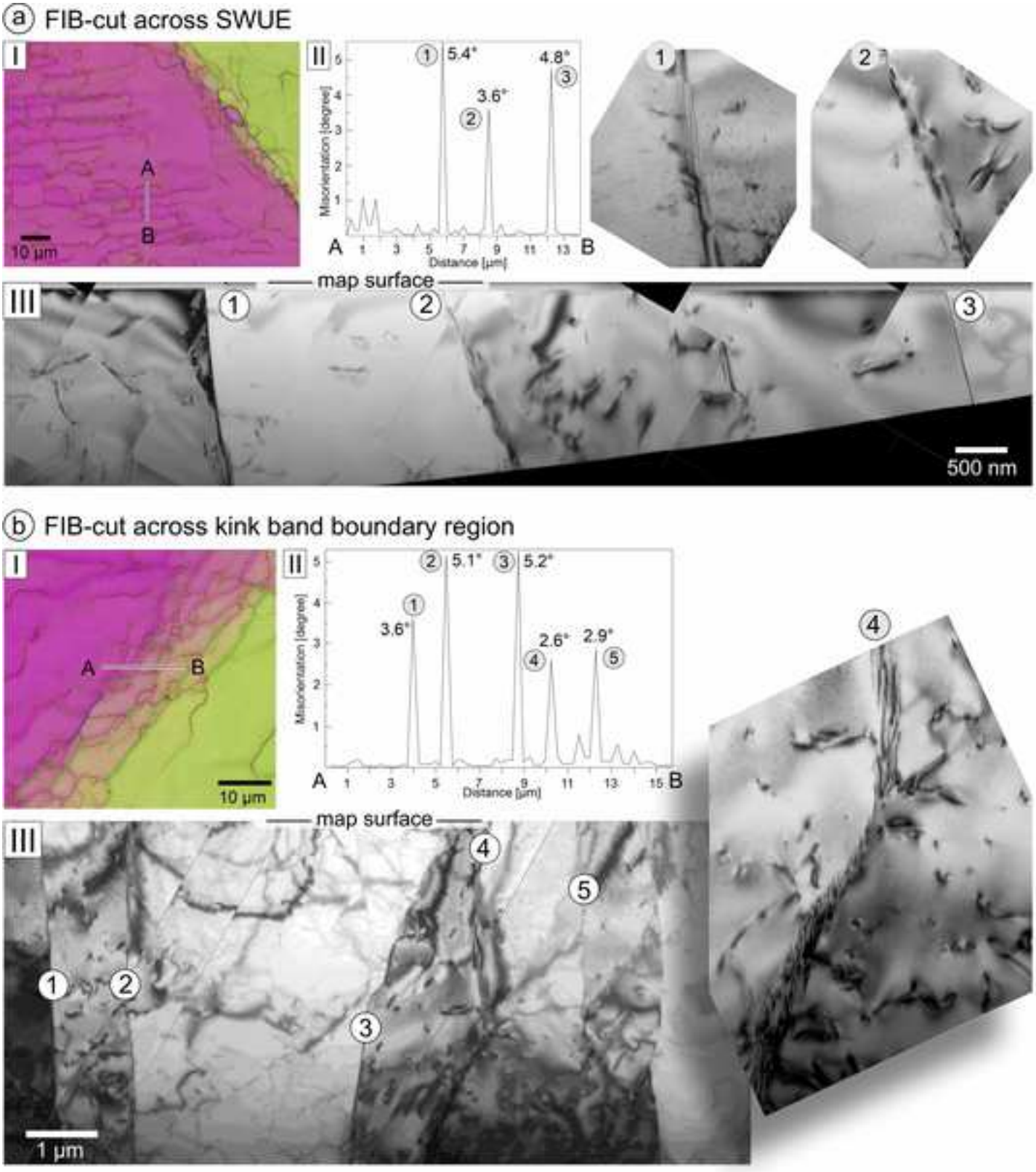

Figure

Click here to access/download;Figure;Fig-7_Bestmann et al_EPSL_submit_kink-micas_red.jpg

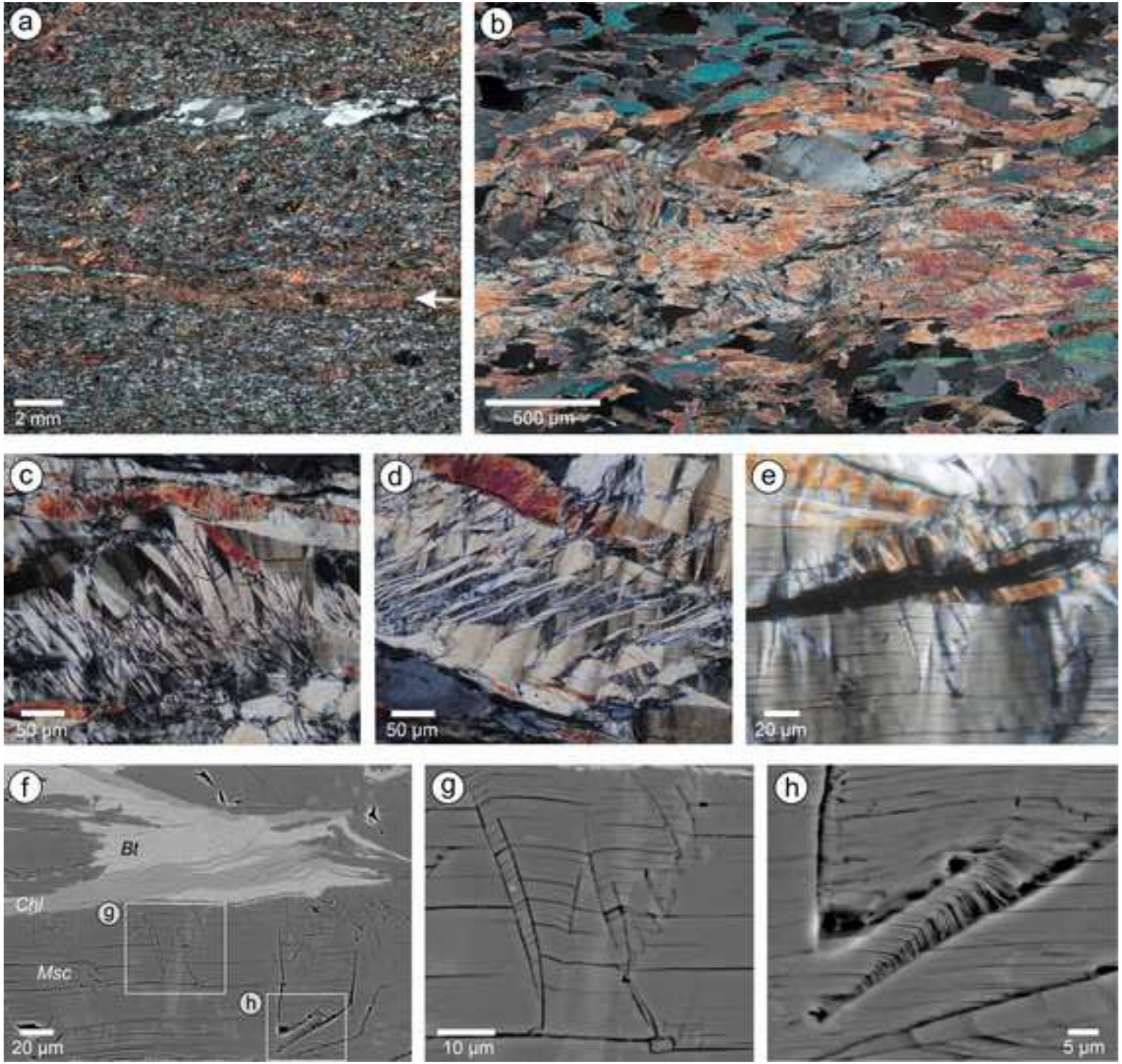

Figure

Click here to access/download;Figure;Fig-8_Bestmann et al_EPSL_submit_kink evolution model_red.jpg

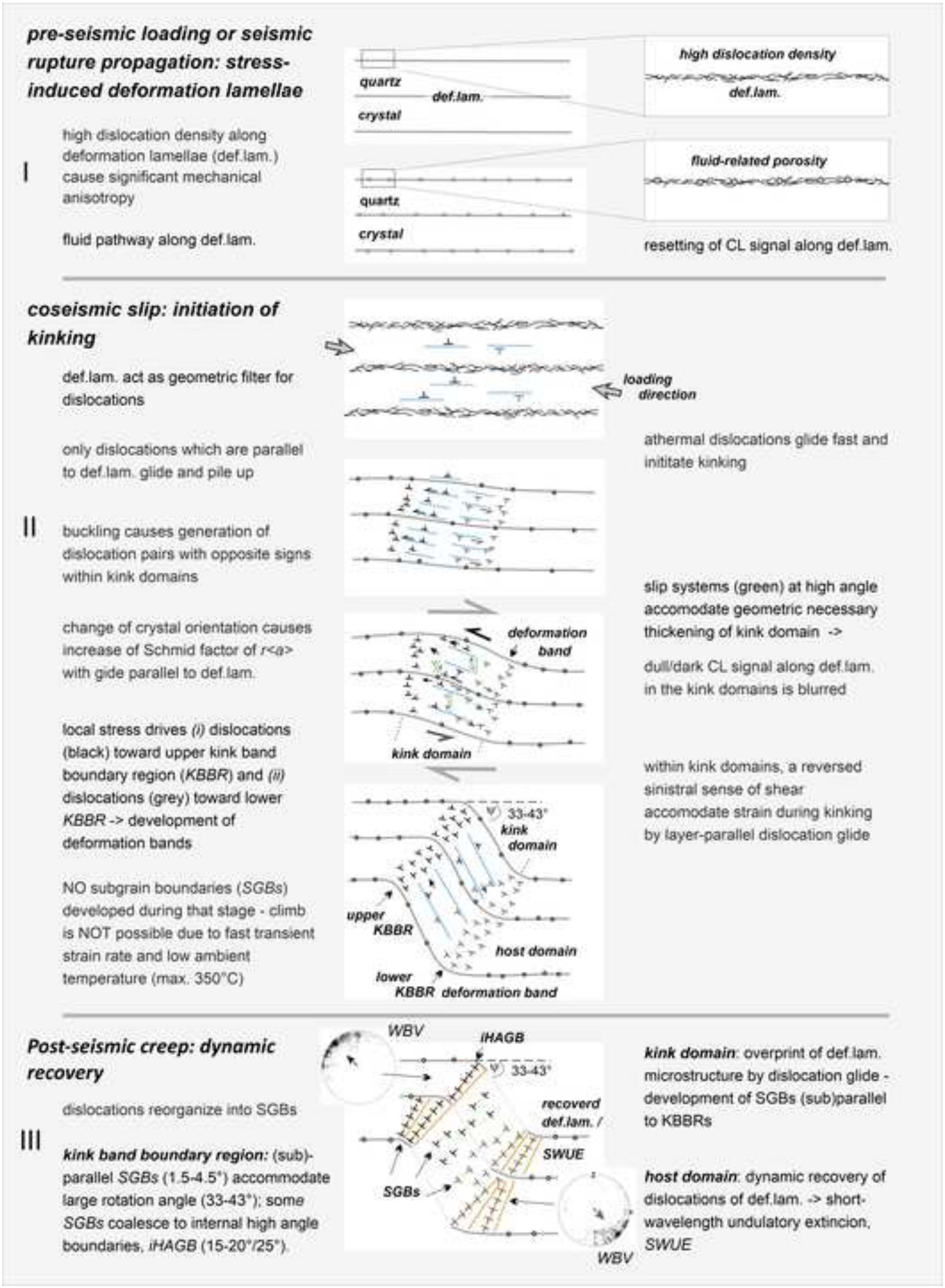

Declaration of interests

☐The authors declare that they have no known competing financial interests or personal relationships that could have appeared to influence the work reported in this paper.

☒The authors declare the following financial interests/personal relationships which may be considered as potential competing interests:

Michel Bestmann reports financial support was provided by German Research Foundation. Bernhard Grasemann reports financial support was provided by Austrian Science Fund. Giorgio Pennacchioni reports financial support was provided by Ministry of University and research of Italy. If there are other authors, they declare that they have no known competing financial interests or personal relationships that could have appeared to influence the work reported in this paper.